

University of Nevada, Reno

EyeSightVR: An Immersive and Automated Tool for Comprehensive
Assessment of Visual Function

A thesis submitted in partial fulfillment of the
requirements for the degree of Master of Science in
Computer Science and Engineering

by

Nasif Zaman

Dr. Alireza Tavakkoli – Thesis Advisor
May 2021



THE GRADUATE SCHOOL

We recommend that the thesis
prepared under our supervision by

Nasif Zaman

entitled

**EyeSightVR: An Immersive and Automated Tool for
Comprehensive Assessment of Visual Function**

be accepted in partial fulfillment of the
requirements for the degree of

Master of Science

Alireza Tavakkoli, PhD
Advisor

George Bebis, PhD
Committee Member

Eelke Folmer, PhD
Committee Member

Mircea Nicolescu, PhD
Committee Member

Michael Webster, PhD
Graduate School Representative

David W. Zeh, Ph.D., Dean
Graduate School

May, 2021

Abstract

The complexity of the human visual system enables the rich sensory immersion we have with our surroundings. When neuro-ophthalmic conditions ail this arrangement, it also affects the function of the eye. For early screening and effective progression monitoring of sight-threatening diseases such as Age-related Macular Degeneration (AMD), glaucoma, and Space-flight Associated Neuro-ocular Syndrome (SANS), the visual function needs to be checked regularly. However, current methods to measure functional health of the ocular system have prominent limitations which include non-conforming lab environments, lack of trained personnel, limited data collection, and uninterpretable perceptual assessments. Furthermore, there is a growing need for a tele-ophthalmic device that would help eye doctors monitor patients remotely. This work surveys current visual function assessment tools that are portable, immersive, and affordable for use in remote, austere, or impoverished areas. We implemented a binocular virtual assessment system that tests different variations of visual acuity, contrast sensitivity, and metamorphopsia in a standardized setting. Additionally, we propose and implement a novel perceptual modeling scheme that uses the Amsler grid to localize, parameterize and suppress the perceived distortion within a wide field of view. We conclude by discussing the crucial limitations of current virtual reality technology that should be addressed in future studies. ...

Dedication

To all the people who have lost their eyesight, your versatility and persistence is my greatest source of inspiration.

Acknowledgments

First and foremost, I would like to thank my thesis Advisor, Dr. Alireza Tavakkoli. Without his guidance and dedicated involvement throughout the process, this work would never have been possible. I am also grateful to our Department of Computer Science and Engineering, UNR. I received a wealth of knowledge and ideas from every class I attended here. I take this opportunity to express gratitude to all of the Department faculty members for their help and support. Without the encouragement and help I received from my lab coworkers, specially Sharif Amit and Lee Easson the process would be considerably more difficult for me. Special thanks to the roommates who have helped create a home away from home. Finally, I owe it all to my family, their unconditional love and support will always drive me forward.

Table of Contents

1	Introduction	1
1.1	Motivation	1
1.2	Problem Statement	2
1.3	Approach	3
1.3.1	VR Calibration	5
1.3.2	VR assessment	5
1.3.3	VR Simulation	6
1.4	Contributions	6
2	Background	8
2.1	Overview of Virtual Reality Systems	8
2.2	Overview of Visual Function Tests	9
2.3	Visual Acuity	10
2.3.1	Procedure for Measuring Visual Acuity with Landolt C Charts	13
2.4	Contrast Sensitivity	14
2.4.1	Gabor Patches	16
2.5	Scotoma and Metamorphopsia	17
2.6	Eye Diseases	18
2.6.1	SANS	19
2.6.2	AMD	21

2.6.3	Effective Strategies	23
3	Related Work	24
3.1	Measuring Visual Function in VR	24
3.1.1	Visual Acuity in VR	25
3.1.2	Contrast Sensitivity in VR	27
3.1.3	Metamorphopsia in VR	28
3.2	Simulating Vision Impairments in VR	29
4	Methodology	33
4.1	Pipeline for Measuring Visual Acuity	33
4.1.1	Far Visual Acuity	33
4.1.2	Measuring Dynamic VA	37
4.2	Pipeline for Measuring Contrast Sensitivity	38
4.3	Simulating Age-related Macular Degeneration	40
4.3.1	Modeling Perceptual Deficit	40
4.3.2	Modeling Scotoma Suppression	47
5	Experiments	49
5.1	Technology	49
5.2	Device Calibration	50
5.2.1	Eye Tracking Calibration	51
5.3	Visual Acuity with VR	51
5.4	Contrast Sensitivity with VR	52
5.5	Suppressing Scotoma in VR	53
6	Conclusion and Future Work	56
6.1	Limitations and Future Work	56

6.2	Future Works	58
6.3	Conclusion	59
7	Appendix	61

List of Tables

3.1	VR in Assessment.	24
5.1	VA result (logMAR) comparison	52
5.2	Parameters tuned to replicate the perceptual deficit caused by AMD	53
7.1	Menu Screen	61
7.2	Response in Static and Dynamic VA test	61
7.3	Response in CS test	62
7.4	Various manipulations for a scotoma	62

List of Figures

2.1	Snellen VA 20/40, denotes that the subject needs to be at a distance of 20 feet to be able to recognize gaps that someone with normal VA can identify from a distance of 40 feet.	11
2.2	A visualisation of the Landolt ring where the size of the gap and feature are equal to 1/5 of the symbol's height.	11
2.3	ETDRS chart based on Landolt C optotypes	12
2.4	Letter height in terms of observer distance	13
2.5	Visual acuity grades, Landolt ring sizes and minimum number of presentations	14
2.6	(a) the parameterization of CSF and (b) visualisation of the CSF dependence on luminance conditions	15
2.7	Three-dimensional (3D) visual field of a normal eye with no defects obtained with 3D computer-automated threshold Amsler grid testing. The X-axis denotes the horizontal visual field in degrees, the Y-axis denotes the vertical visual field in degrees, and the Z-axis depicts the contrast sensitivity as a function of location (X, Y).	17
2.8	Direct and Indirect Indications of SANS sign	19
2.9	Different perceptual impacts of AMD on vision	22
4.1	Continuous sampling of Gap size from curve	34

4.2	Conversion between different types of VA measures [1]	36
4.3	Low vision Acuity equivalent [1]	37
4.4	Conversion between contrast sensitivity metrics [1]	38
4.5	Changing stimuli spatial frequency and contrast	39
4.6	Simulating perceptual deficit	41
4.7	Illumination Degradation Γ , represented by the proposed parametric model	42
4.8	Perceptual deficit region Ω , represented by the proposed parametric model. The area within the solid blue region represents illumination degradation of more than λ percent.	43
4.9	Different perceptual deficit region Ω at different boundary strength λ . The area within the solid blue, green, and red regions represents decreasing boundary strength of $\lambda = 18\%$, $\lambda = 12\%$, and $\lambda = 5\%$, respectively.	44
4.10	Modeling rotational distortion: (a) A single Gaussian kernel illumination degradation. (b) The perceptual impact regions with $\lambda = 0.5$. (c) the Rotational distortion with $\pi/2$ angle. (d) Both illumination degradation and rotational distortion.	45
4.11	: Vector fields representing the spatial distortion maps, as modeled by: (a) a single Gaussian kernel, and (b) multiple Gaussian kernel	46
4.12	Spatial distortion of the Amsler grid as represented by the Ψ component of the proposed model. Note the model adaptation and its ability to capture disease progression: modeling spatial distortion with (a) a single Gaussian kernel, (b) two Gaussian kernels, and (c) three Gaussian kernels.	47

4.13	Rotational distortion and illumination degradation as the disease progresses.	48
5.1	HTC Vive Pro Eye System	49
5.2	Calibration of the Headset(a) Interpupillary distance (b) Lenses . . .	50
5.3	This shows what participants see when they wear the VR headset. In (a) the left eye sees an Amsler grid with simulated distortion and the right eye sees it without distortion. In (b) a small suppression is introduced to the distortion. (c) and (d) show a gradual increase in the suppression size.	55
7.1	Overview of the Metamorphopsia Implementation	63
7.2	Start Screen	64
7.3	Main Menu	64
7.4	Binocular Static Visual Acuity	65
7.5	Binocular Dynamic Visual Acuity	66
7.6	Contrast Sensitivity Test	67

Chapter 1

Introduction

1.1 Motivation

Assessment of vision is the first step in ophthalmic care and often requires sophisticated equipment and specialized clinical expertise. Proper ophthalmic evaluation and care employ these equipment and clinical expertise in the earlier stages of disease progression to ensure the best outcomes [2]. In many cases (e.g. retinal detachment) rapid diagnosis and immediate treatment can prevent permanent vision loss. This highlights the need for early assessment and screening for any vision alterations even in remote and austere environments. Unfortunately, traditional ophthalmic resources are not sufficiently prevalent in most parts of the world. Despite the urgent need to have comprehensive medical consultation with an eye surgeon immediately after vision alterations are noticed, ophthalmology services and ophthalmic care are available only at the highest echelon of care in large cities or advanced medical facilities. Even more pressing is the very limited state of practice in teleophthalmology, i.e. via phone or video conference with an eye surgeon. Even in the most urgent cases, the

information available via video conferencing is limited to pictures of the eye and self reported symptoms. This prevents robust evaluation of potentially vision threatening injuries for patients who do not have convenient access to ophthalmology services, putting the patient's vision at risk of irreparable loss.

Functional assessments such as visual field perimetry (VF) [3], color and contrast sensitivity [4], and visual acuity [5] provide measures of visual ability and are widely used for preliminary screening and monitoring. Unfortunately, traditional functional assessments have strict requirements that are difficult to meet. These tests are carried out in person and require a controlled environment, effective visual stimulation and attentive response to yield reliable results. Complicating the issue further, these results are highly subjective and lack the diagnostic power of more expensive but reliable ocular imaging technologies such as optical coherence tomography (OCT), fluorescein angiography (FA), and fundus imaging. All of these challenges motivate our search for a novel medium to conduct vision screenings in a more equitable and accessible manner. Virtual Reality (VR), with its affordable set of all-round visualization and interactive capabilities is a promising new tool for ophthalmic care. VR can reduce gap in telemedicine for ocular health, especially for populations with limited resources and access to comprehensive ophthalmology services. It can provide early screening and more frequent monitoring to the aging communities all around the globe.

1.2 Problem Statement

VR creates safe, manageable, and life-like environments that allow study subjects to behave as they would in a real-world scenario. VR environments are ideal for studying visual impairments as they offer researchers comprehensive control over user experi-

ence and stimuli. For instance, dichoptic rendering in VR allows researchers to assess participants' monocular vision by presenting varying stimuli to eyes independently. Moreover, external illumination has no effect on such assessment outcomes as the user is visually isolated from external stimuli. In addition, using head and eye tracking in VR provides correction for fixation and attention loss. All of these advantages have led us to explore the viability of visual function tests in VR as an alternative to traditional tests. To test the effectiveness of such a system, we chose to include the most widely assessed visual functions: visual acuity (VA), contrast sensitivity (CS) and visual distortion (metamorphopsia). We adapt these physical tests to an intuitive, immersive and inexpensive virtual medium by answering the following questions:

- Q1: How to detect and quantify important aspects of visual function with variations in Visual Acuity tests?
- Q2: How to measure contrast sensitivity in a VR environment?
- Q3: How to model and quantify the perceptual error in a scotomatous eye with Amsler grids?

We hypothesize that answering these questions would lead to a comprehensive visual assessment tool that can provide ophthalmic services to remote areas with scarce resources.

1.3 Approach

Many eye practitioners use VA to determine the overall visual abilities of their patients. Visual acuity is extensively used in both comprehensive and problem focused eye exams where visual defects from ocular disease (e.g. diabetic retinopathy) or refractive error (e.g. myopia) are suspected. However, the most common variation

of VA, known as distant VA does not always reveal the full story of a patient’s visual abilities. Additional information can be obtained from testing eyes separately, and under different motion conditions. Other vision tests such as contrast sensitivity (CS) are often used in combination with visual acuity to gain a better understanding on quality of life [6]. Contrast sensitivity is an individual’s ability to distinguish an object from its background using luminance as a cue. This is often used to help with everyday mobility tasks like navigating through a room or telling the difference between the sidewalk and street [6]. Many practitioners test both VA and CS on their low-vision patients, but only test VA on their normal-sighted patients. Contrast sensitivity testing used to have a reputation for being too unreliable, too difficult to test, and unrelated to quality of life [7]. However, past and current research has established standardized methods for testing that are easier for examiners to use, provide more reliable data, and show how the impact these conditions have on the quality of life. Still, under very subjective conditions, such as perceptual loss caused by scotomatous regions in the central visual field due to Age-related Macular Degeneration (AMD), can be very tricky to assess. In this thesis, we present a methodology to model these perceptual functions alongside standardized, quantitative visual function tests to offer comprehensive visual assessment in a portable VR system. Our methodology describes how to conduct these tests in a standardized manner that ensures the reliability of the acquired data along with the ease-of-use of the participants. We consider adjustments to the test procedure where it can improve the user experience. We leverage most of the advantages of a state-of-the-art VR and eye tracking to ensure that the results are only measures of visual function and are not biased by inattention, distraction, non-standard conditions, etc.

We present a methodology that comprises a calibration step, four different visual function tests that measure different aspects of user perception and then a composite

pipeline that simulates the modeled deficits for validation.

1.3.1 VR Calibration

In order to properly utilize the virtual assessment, the environment would need to be calibrated at the beginning of each session. Simple calibrations such as adjusting lens distance, interpupillary distance and headset adjustments are done at the start. After these adjustments, the fixation and tracking capabilities of the eyes are tested, first binocularly and then monocularly. These performance metrics are saved alongside the user demography information.

1.3.2 VR assessment

After the calibration phase, the user's visual assessment can commence. Visual acuity, contrast sensitivity and visual distortions are assessed through a variety of procedures. For VA, binocular distant VA as well as dynamic VA is measured under mesopic (natural light) conditions. Instead of using images of conventional charts, we render individual characters in front of the user at predetermined distances and scale it based on user response. The results are reported in logMAR scale among others.

The contrast sensitivity is measured using gabor patches as stimuli. In this test, the user gaze follows a gabor patch that alters its contrast and spatial frequency based on user performance. At the end, the contrast sensitivity expressed in logCS among other contrast sensitivity units.

The amsler grid test is adapted to VR to measure the perceptual distortions in AMD patients. At the start of the exam, the amsler grid is displayed in front of both eyes. While looking at a fixation point in grid, if the straight grid lines appear to be distorted the user emulates the metamorphopsia of the deficient eye on the healthy

eye. This grid manipulation is modeled as a gaussian mixture of different scotoma parameters. The results are reported as the image of the altered amsler grid.

1.3.3 VR Simulation

The collected results for each of the visual assessments are then used to create a simulation of the perception of the user. This pipeline combines results from all of the tests to offer a single visualization. For example, lower visual acuity values would lead to the scene appearing blurry and the existence of scotomas would create distortions in the scene. The saved parameters can be pulled up at any time so that others can experience the perceptual loss measured by all three tests individually and collectively.

1.4 Contributions

The main contributions of this thesis can be summarized as follows:

- VR Calibration
 - Our system enables us to calibrate the virtual environment settings. We take into account a user’s capabilities and preference, as well as hardware constraints of the VR HWD and is based on medical eyesight tests.
- VR Assessment
 - We introduce a novel methodological framework for assessing and modeling aspects of vision.
- VR Simulation

- The model parameters are then used to partially model and counter the perceptual loss of the participant for validation.

Chapter 2

Background

2.1 Overview of Virtual Reality Systems

A participant in virtual reality (VR) perceives a world that does not exist. This is generally achieved by presenting computer generated images through a binocular head-mounted display (HMD) to invoke sensory immersion [8]. However, to create high-fidelity immersion, the individual eyes need slightly different view of the scene. In order to produce this binocular disparity artificially, the 3D computer generated scene is projected onto two virtual cameras. These cameras are placed interpupillary distance apart. These virtual projections are then perceived as a single 3D scene by the viewer, forming the immersive VR environment [9]. In addition to binocular disparity, VR technologies use several other visual cues such as motion parallax [8,10], a monocular depth cue arising from the relative velocities of objects moving across the retina of a moving person [11].

This realism has vaulted research into human behavior and psychophysics [12–14]. The safe, manageable, and life-like VR environments allow study subjects to

behave naturally. VR environments are also ideal for simulations of a diverse set of perceptual impairments. Researchers can exercise considerable control over user experience and scene presentation. For instance, dichoptic rendering in VR allows researchers to assess participants' monocular vision by presenting varying stimuli to each eye independently. Moreover, external illumination has no effect on the assessment outcome as the user is visually isolated from external stimuli. In addition, when eye tracking is used alongside VR, it can indicate loss in fixation or attention during assessment. Therefore, it is not surprising to see researchers use VR to study human vision in novel ways.

VR based telemedicine and diagnostics has key advantages that computer-based solutions cannot provide: full-field immersion, isolation from external factors such as illumination and stimuli placement, comprehensive control over stimuli properties, and portability. Most importantly, virtual reality can influence the perception of a person to a greater degree than is possible by computer displays. Furthermore, even commercial-off-the-shelf VR headsets such as FOVE0, HTC Vive Pro Eye, now come with eye-tracking that greatly enhance the assessment process. When coupled with visual function tests that leverage the strengths of virtual reality, the results can be significantly more informative. Furthermore, uniting multiple types of functional tests under one VR-based system reduces the overhead hardware, training, setup and calibration time.

2.2 Overview of Visual Function Tests

Multiple structurally and functionally overlapping constituent pathways conjoin to form a specialized and hierarchical visual system. Light sensitive photoreceptors and ganglion cells respond to specific spatial and temporal frequencies of stimuli. Optic

nerve carries visual information to the visual cortex, where several segments of the brain selectively process different portions of the captured image. The capabilities of these mechanisms may be selectively impacted as a result of different developments, degeneration, and vulnerabilities [15]. The complicated organization of the visual system means that in order to characterize visual performance in a comprehensive manner, multiple tests must be carried out to assess the functioning of different visual structures and pathways. Practical testing limitations related to instrumentation and the demands placed on a participant, coupled with challenges associated with testing unique clinical populations, has led to an evolution and refinement of the assessment methods employed. Two of the most informative visual function outcomes are visual acuity and contrast sensitivity. Metamorphopsia is less commonly tested but has proved to be a reliable indicator of macular function and complication [16]. In the next subsections we explain how each of these measures are taken and what those measurements mean.

2.3 Visual Acuity

VA quantifies the ability of a person to recognize small visual details. In clinical settings, it is measured by presenting the different standardized symbols called optotypes, such as the Landolt C at varying sizes. Based on the minimum size at a predefined distance, and determining which size can be recognized. VA is usually expressed relative to 20/20, the Snellen fraction for the test distance of 20ft, or 6/6 in meter, or the decimal, or logarithm value of these fractions. This is illustrated in the [Figure 2.1](#) In the fractional representation the numerator specifies the viewing distance (20 feet) at which a person who is tested can recognize the same size of optotypes as a person with normal sight (20/20) can from the distance given by the

denominator.

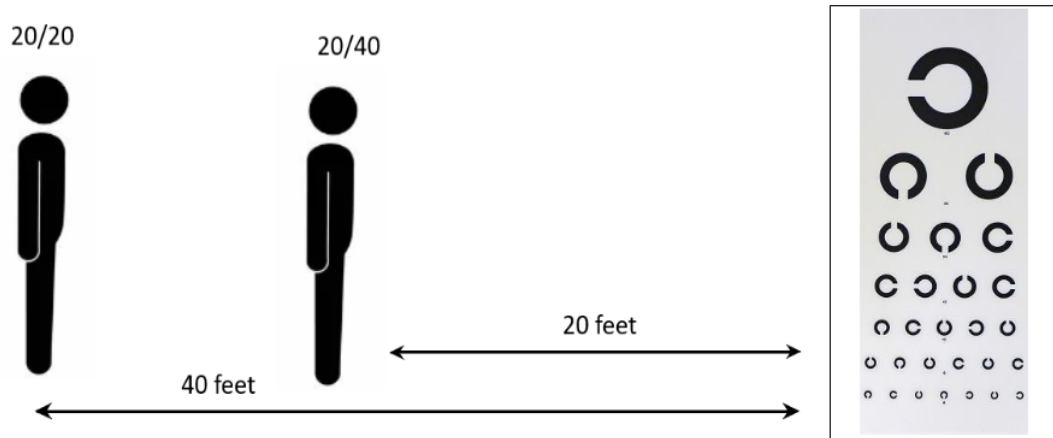


Figure 2.1: Snellen VA 20/40, denotes that the subject needs to be at a distance of 20 feet to be able to recognize gaps that someone with normal VA can identify from a distance of 40 feet.

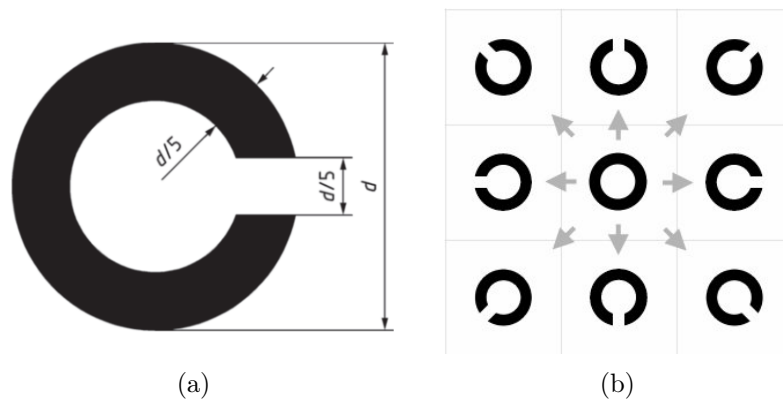


Figure 2.2: A visualisation of the Landolt ring where the size of the gap and feature are equal to $1/5$ of the symbol's height.

Normal vision is classified as the ability to recognize a detail that spans 1 arc minute ($1/60$ of a degree). This can theoretically be tested at any viewing distance as long as the detail in question is appropriately scaled in relation to the distance. However, nearsighted people can see very close objects well and only have a reduced VA at a certain distance. Therefore the test distance should not be too short (e.g. not under 1 meter). Measuring VA at 20 feet is considered standard [17].

ISO 8596 also defines LogMAR acuity as the logarithm (base 10) of the minimum angle of resolution in minutes of arc. Consequently, the decimal acuity value dA can be computed from the LogMAR value lM as:

$$dA = 10^{-lM} \quad (2.1)$$

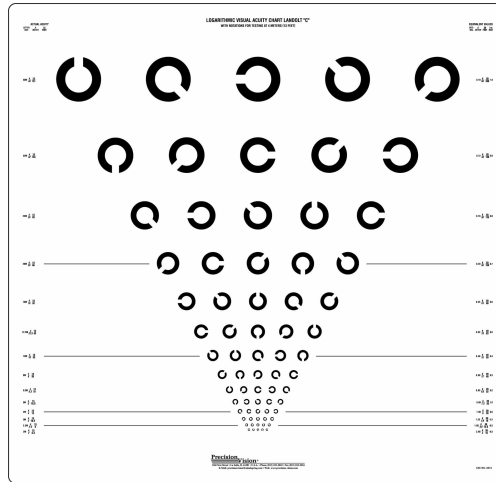


Figure 2.3: ETDRS chart based on Landolt C optotypes

Next, we describe how visual acuity charts, specially the ETDRS Landolt C chart can be used to measure VA.

2.3.1 Procedure for Measuring Visual Acuity with Landolt C Charts

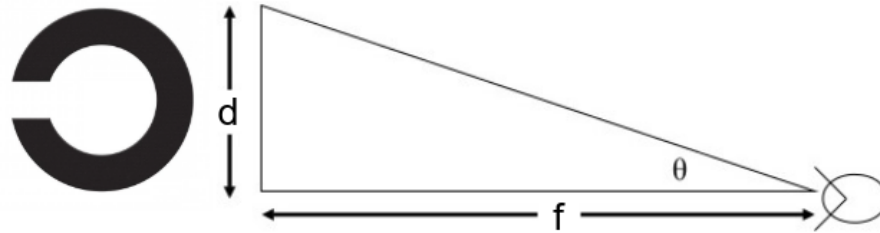


Figure 2.4: Letter height in terms of observer distance

Each row of the ETDRS chart [Figure 2.3](#) contains letters that are 0.1 logMAR off from adjacent rows. The actual size of the letters (d) in the metric system is calculated using the stimuli visual angle (θ) in minutes of arc, and the distance between the person and the eye chart (f). Based on figure [Figure 2.4](#), the relationship between these values can be expressed as:

$$\tan(\theta) = d/f \quad (2.2)$$

The ISO standard ISO 8596 also defines orientation of the test symbols and procedures to determine a subject's VA under daytime conditions (200 cd/m^2), devoid of any visible glare or reflection from surfaces within the field of view. The gap size and the thickness of the ring are defined in terms of the diameter of the ring [Figure 2.2\(a\)](#). The position of the gap should be horizontally left or right, vertically up or down or diagonally in-between for a total of eight possible positions [Figure 2.2\(b\)](#).

To find the visual acuity of a person, they start on the last row where they can read all of the letters, and then read down until they reach a row where a minimum of three lines cannot be read. That row determines their visual acuity.

Visual acuity grades (nominal values) ^d			Gap size of Landolt ring (minutes of arc)	Minimum number of presentations ^d
Decimal visual acuity ^a	LogMAR acuity	Snellen fraction for test distance 6 m		
0,05	+1,30	6/120	20,0 ^b	2
0,063 (0,06)	+1,20	6/95	15,8 ^b	2
0,08	+1,10	6/75	12,6 ^b	2
0,10	+1,00	6/60	10,0 ^b	2
0,125	+0,90	6/48	7,94 ^b	3
0,16	+0,80	6/38	6,31 ^b	3
0,20	+0,70	6/30	5,01 ^b	3
0,25	+0,60	6/24	3,98 ^b	5
0,32 (0,30)	+0,50	6/19	3,16 ^b	5
0,40	+0,40	6/15	2,51 ^b	5
0,50	+0,30	6/12	2,00 ^b	5
0,63 (0,60)	+0,20	6/9,5	1,58 ^b	5
0,80	+0,10	6/7,5	1,26 ^b	5
1,00	0	6/6,0	1,00 ^b	5
1,25	-0,10	6/4,8	0,794 ^b	5
1,60	-0,20	6/3,8	0,631 ^b	5
2,00	-0,30	6/3,0	0,501 ^c	5

^a The values in parentheses shall be used only for the purpose of identifying the acuity grade.

^b The gap size is accurate to 1 %. The permissible deviation is 5 %.

^c The permissible deviation is 10 %.

^d The recommended number of presentations is at least 5 presentations.

Figure 2.5: Visual acuity grades, Landolt ring sizes and minimum number of presentations

2.4 Contrast Sensitivity

While visual acuity measures the smallest perceivable cues, its testing utilizes full black targets presented on a white high contrast background. However, our natural surroundings contain objects at multiple sizes and luminosity intensities. Differences in image intensity are quantified by contrast (typically the difference between the lightest and darkest features in an image divided by the mean intensity), and differences in size are quantified by spatial frequency (the reciprocal of the retinal distance between light or dark image regions in degrees of visual angle [Figure 2.6\(a\)](#)). Contrast

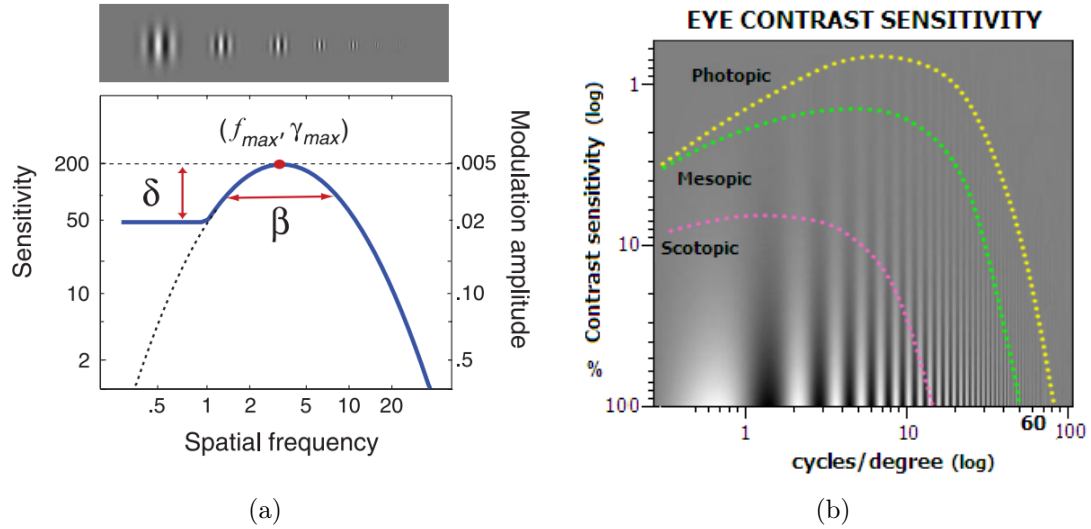


Figure 2.6: (a) the parameterization of CSF and (b) visualisation of the CSF dependence on luminance conditions

sensitivity is the inverse of the smallest contrast required for recognition, and is highly dependent on spatial frequency. This relationship between spatial frequency and contrast sensitivity is called the Contrast Sensitivity Function. It is important to note that contrast sensitivity has been shown to be a better measure than visual acuity in terms of predicting performance on activities of daily living and the detection of real objects [18].

Contrast sensitivity can be measured with sine wave grating patches presented at several spatial frequencies. The contrast sensitivity function, $S(f)$, represents sensitivity ($1/\text{contrast}$) as a function of grating frequency (f). Based on a review of nine parametric functions, [19] concluded that all provide a roughly equivalent description of the standard CSF. The truncated log-parabola Figure 2.6(a), describes the CSF with four parameters: (1) the peak gain (sensitivity), γ_{max} ; (2) the peak spatial frequency, f_{max} ; (3) the bandwidth β , which describes the function's full-width at half-maximum (in octaves), and (4) δ , the truncation level at low spatial frequencies.

Without truncation, the log-parabola, $S'(f)$, defines (decimal log) sensitivity as:

$$S'(f) = \log_{10}(\gamma_{\max}) - \log_{10}(2) \left(\frac{\log_{10}(f) - \log_{10}(f_{\max})}{\log_{10}(2\beta)/2} \right)^2 \quad (2.3)$$

From a clinical standpoint, it is important to realize that a given type of visual impairment can selectively affect the visibility of only a specific range of spatial frequencies. For example, the detection of high spatial frequencies is impaired in uncorrected refractive error and amblyopia. Medium spatial frequencies are selectively impaired in Parkinson's disease. Finally, cataracts have been shown to selectively impair the detection of low spatial frequencies. This means that the comprehensive assessment of contrast sensitivity requires measurement at several spatial frequencies in order to detect any potential deficits related to both detection and resolution ability.

2.4.1 Gabor Patches

The typical building block of the visual stimulus in contrast sensitivity tests is a Gabor patch, which efficiently activates and matches the shape of receptive fields in the visual cortex. The following equation is widely used to generate gabor patches:

$$g(x, y; \lambda, \theta, \psi, \sigma, \gamma) = \exp\left(-\frac{x'^2 + \gamma^2 y'^2}{2\sigma^2}\right) \cos\left(2\pi \frac{x'}{\lambda} + \psi\right) \quad (2.4)$$

where,

$$x' = x \cos \theta + y \sin \theta$$

$$y' = -x \sin \theta + y \cos \theta$$

In [Equation 2.4](#), λ represents the wavelength of the sinusoidal factor, θ represents

the orientation of the normal to the parallel stripes of a Gabor function, ψ is the phase offset, σ is the sigma/standard deviation of the Gaussian envelope and γ is the spatial aspect ratio, and specifies the ellipticity of the support of the Gabor function.

2.5 Scotoma and Metamorphopsia

Metamorphopsia is a subjective visual disorder which can spatially distort the subject's perception beyond repair. Crucially, it is reported that metamorphopsia may adversely affect daily vision related activities, including reading and recognizing faces [20]. While the severity of metamorphopsia can be self-evident to sufferers, the ramifications of the inability to express or exhibit metamorphopsia may cause further problems, including the monitoring of patients' medical treatment, vision rehabilitation strategies, or even litigation situations. However while qualitative measures surface in metamorphopsia depiction, expression of quantitative measures of metamorphopsia in the context of perceptual depiction has yet to be explored.

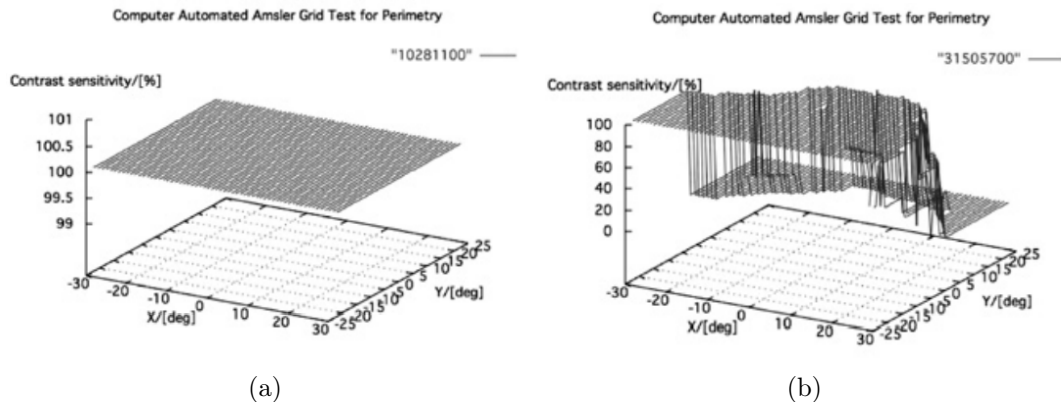


Figure 2.7: Three-dimensional (3D) visual field of a normal eye with no defects obtained with 3D computer-automated threshold Amsler grid testing. The X-axis denotes the horizontal visual field in degrees, the Y-axis denotes the vertical visual field in degrees, and the Z-axis depicts the contrast sensitivity as a function of location (X, Y).

The Amsler grid was developed by Marc Amsler [21] in the 1940s to test and analyze visual field defects in the central 10 degrees (3, 4) using a suprathreshold target. It was designed to detect scotoma and metamorphopsia, but is not as sensitive for the detection of relative scotoma. Relative scotoma is a region of visual field loss where there is some residual light perception left. Amsler grid is an alternative to central VF analysis if a swift assessment of macular function is required, and it is particularly useful in cases with metamorphopsia or visual distortion. It is a grid of horizontal and vertical lines used to visualize the distorted perception of an individual. The 3-D Computer-Automated Threshold Amsler Grid Test depicted in [Figure 2.7](#) is a variation of this perceptual test [22]. It is performed on a laptop computer with a touch sensitive screen that takes about five minutes per eye to complete. With one eye covered, a person sits in front of a computer screen divided into a grid. The subject stares at a central spot on the touch-sensitive screen and, using a finger, outlines missing areas of the grid. The same procedure is then repeated at various greyscale levels - simulating increasing degrees of contrast - and the respective results are recorded and later automatically displayed by the computerized test program. However, the test is highly subjective, and the reliability is contingent upon constant fixation.

2.6 Eye Diseases

Vision impairment presents as a significant detriment to an individual's quality of life [23] and is highly prevalent across the globe with approximately 43 million individuals recognized as blind [24]. Compared with the general population, adults with visual dysfunctions often have lower rates of workforce participation and productivity [25] and higher rates of depression and anxiety [26]. It has been shown that

vision impairment in older adults contributes to social isolation [27], increased risk of physical injuries [28] –particularly hip fractures [29], and a greater likelihood of early entry into nursing or assisted living facilities [30].

2.6.1 SANS

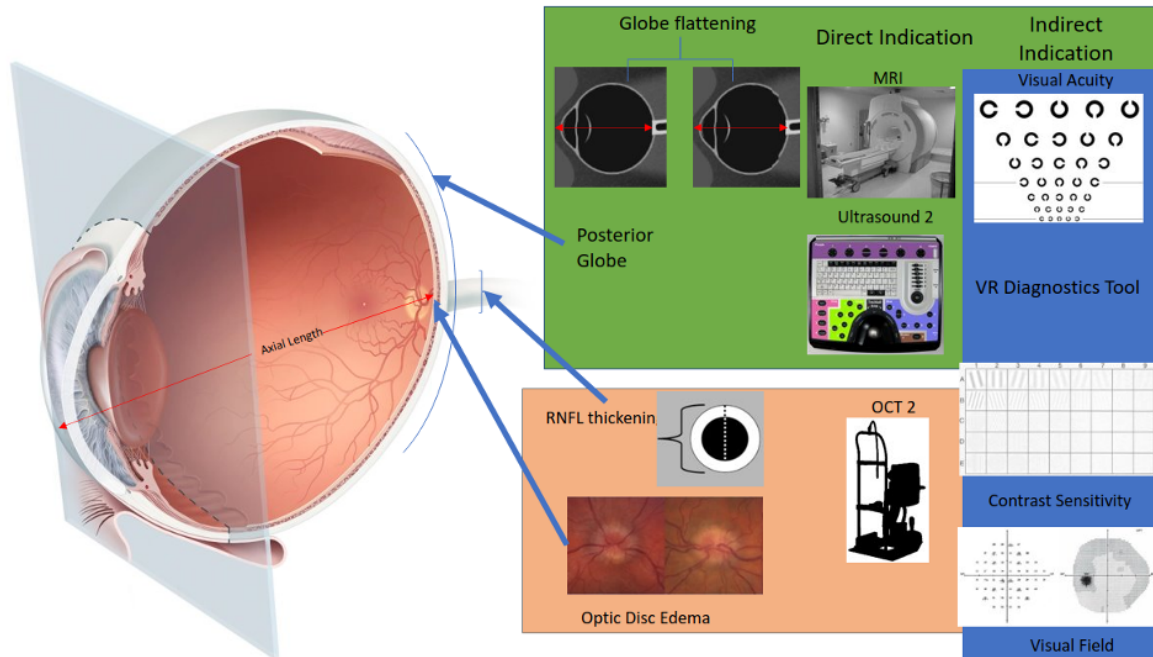


Figure 2.8: Direct and Indirect Indications of SANS sign

Visual impairment is one of the most impactful health risks for astronauts. VIIP and more recently Spaceflight Associated Neuro-ocular Syndrome (SANS) study has gained considerable attention because impairment to human vision due to microgravity can jeopardize spaceflight. Novel neuro-ophthalmic findings indicate that SANS may be the end result of cephalad fluid shifts to the brain and orbit brought about by extended microgravity exposure. There have been various other candidate models to explain the structural and functional ocular changes in astronauts during LDSF. Researchers have used ocular structure-function, biochemical analysis of proteomes under spaceflight and artificial gravity to invalidate old models and propose new ones.

Still, many SANS-related mechanisms remain unknown. The full impact of microgravity on ocular physiology and function have not been measured. Moreover, even an objective measurement criterion sensitive to SANS monitoring is yet to be devised. Understanding the mechanism behind SANS is imperative to devising a satisfactory countermeasure that would ensure normal neuro-ophthalmic function during LDSF.

However, there are logistical hurdles to collecting enough data to aid in SANS investigation. For instance, the Space Medicine Operations Division of NASA can only manage a total of 30lb medical equipment and supplies [31]. This means they must cautiously choose the number, frequency, and extent of future medical exams. Additionally, the limited time an LDSF astronaut spends in the space station is highly packed with activities critical to various other scientific studies. Therefore, in-flight ocular data collection is restricted to preset intervals of L+30, 90, 180, 270, R-30 days [32]. The complexity of the visual pathway coupled with the relative scarcity of available in-flight data make it difficult to resolve the mechanisms behind SANS. Therefore, terrestrial analogs were created and are being examined to gain insight on SANS. Such terrestrial analogs can be used to establish relations between visual function and changes to ocular structure. This approach would be especially valuable since traditional visual function tests available in the International Space Station (ISS) don't require an additional operator and can be completed more quickly compared to ocular imaging tasks such as fundoscopy, OCT, ultrasound. Moreover, recently developed visual function tests are faster than their traditional counterparts, yet equally reliable. This makes vision assessments such as visual acuity, color vision, contrast sensitivity, perimetry, and metamorphopsia highly complementary to Neuro-ophthalmic imaging modalities for SANS monitoring.

Once ocular structures such as Optic Disc Edema, Choroidal Folds, Optic Nerve Sheath Diameter increase, Cotton Wool Spots etc. can be predicted using results from

visual function tests, it would be substantially easier to investigate SANS etiology and progression. There are lots of tools to precisely and objectively model individual eyes with considerable precision, but all of them would not be suitable for inflight assessment. The versions of assessment tools available in the ISS were chosen because of their portability and reliability. Therefore, in this study we have limited ourselves to solutions that are portable or can be implemented in a compact system. Virtual Reality is a simulated environment that facilitates highly controllable environments, stimulus and interaction. Therefore, we have specifically focused on VR-based assessments already in the literature. We hypothesize that our VR-based implementation of the latest visual function testing techniques will greatly aid in SANS research.

2.6.2 AMD

Age-related Macular Degeneration (AMD) is the leading cause of irreversible blindness and visual impairment in otherwise healthy individuals in the U.S. There are two basic forms of AMD: “Wet AMD” and “Dry AMD”. Dry AMD will typically cause a chronic loss of central vision. In wet AMD, the affected individual may notice distortions of central vision, known as metamorphopsia. A patient with metamorphopsia complains that lines, which should appear straight, are wavy. The central vision loss and metamorphopsia are among a plethora of vision deficits caused by neuronal degeneration and neural errors. Although compensation for optical errors, e.g. myopia or hyperopia, has a very long and successful history [33], compensation for neural errors is still in its infancy and requires advanced techniques for processing input images and novel methodologies for characterizing visual losses. One of the main barriers impeding progress in this area is the lack of understanding the nature, and the extent, of correlations between ocular physiology and visual function.

Despite years of attempt to develop visual prosthesis to recover lost vision, the



Figure 2.9: Different perceptual impacts of AMD on vision

vision restored by retina and visual cortex implants such as, Argus II, Epi-Ret 3, and Alpha-IMS (Retina Implant AG) is merely “moving shadows” [34]. A recent study concluded that these prostheses suffer from the fundamental reorganization of the degenerated retina [35]. New techniques such as opto genetics [36] are likely to face many of the same issues related to integration and propagation of artificially created neural patterns of activity into a useful visual percept [37]. In addition to these limitations, visual prosthetics require complicated microsurgery and may not be suitable as a first-line treatment for patients without complete loss of vision. As a result of these limitations in visual prosthetics, enhancing the remaining vision for patients suffering from neural conditions is of utmost importance.

As we have noted in the section on metamorphopsia, the main problem is the difficulty in interpreting the perceptual impact of the physical damage. For example, AMD can cause a number of different perceptual effects in patient’s vision, as shown in [Figure 2.9](#). Therefore, the main question to address in developing a model of perceptual deficit is, what does the patient see as a result of the physical damage to the retina, and can we correct it?

2.6.3 Effective Strategies

A range of effective strategies are available to address the needs associated with eye conditions and vision impairment across the life course. These include health promotion, prevention, treatment and rehabilitation strategies, some of which are among the most feasible and cost-effective of all health care interventions to implement. Nonetheless, progress is not keeping pace with population eye care needs of approximately 295 million people who have moderate to severe vision impairment [24]. Major challenges lie ahead. Firstly, With an aging population, it is estimated that these numbers would significantly increase by 2050 [24]. Secondly, eye care facilities and available workforce is inadequate to handle such increasing numbers. Thirdly, data are often lacking and health information systems weak, thus hampering planning. Therefore, we need a visual assessment tool that can address all of these concerns.

Chapter 3

Related Work

3.1 Measuring Visual Function in VR

Table 3.1: VR in Assessment.

Test	Contributors	Hardware	Software	Track	N
Visual Acuity	[38]	Virtual Research Flight Helmet	WorldToolKit	✗	24
	[39]	HTC Vive and Oculus Rift	Unity	✗	1
	[40]	HTC Vive Pro and Oculus Rift	Propriety	✗	8
	[41]	HTC Vive Pro	Unreal Engine 4	✗	15
	[42]	Epson Moverio B350	Android Studio	✗	60
	[43]	Oculus Rift	Virtual Desktop	✗	22
CS	[40]	HTC Vive Pro and Oculus Rift	Propriety	✗	8
Amsler	[44]	HTC Vive Pro	Unreal Engine 4	✗	n/a
	[45]	HTC Vive Pro	Unreal Engine 4	✗	3

3.1.1 Visual Acuity in VR

Visual acuity (VA) is the measure of an individual's ability to resolve fine details in visual cues [46]. This is an extremely useful ability which facilitates face, letter, sign and feature recognition at a distance. There are two types of VA tests: Static and Dynamic. Static VA is measured by showing the subject stationary, high-contrast alphanumeric symbols of different sizes at a predefined distance. These alphanumerals or clinical optotypes are generally designed and presented at a distance of 20 feet. Someone who is able to discern an optotype that spans 1.75mm at such a distance is considered normally-sighted. When optotypes are mobile with respect to the subject, the test is called dynamic visual acuity. Dynamic VA measures the eye's spatial resolution as well as the function of the oculomotor system. It is one of the best predictors of success in sports [47].

Static VA is widely used even outside the clinical settings, to determine level of disability, fitness for specific jobs, etc. VEPAB [38] was similarly non-clinically motivated to measure individual visual performance in a virtual training environment. VA was one of the metrics they used, by sending 24 participants down a 20-ft virtual corridor that had a Snellen chart at the end. At each 1-ft interval, the number of lines visible to the participant was noted. The study reports a mean acuity of 20/860 which is significantly low compared to the acuity limit of 20/250 imposed by the display density (4.05 ppd). During their pilot testing, the authors experimented with black and white stripes of different orientations to measure the acuity but found that stripes would often disappear into solid fields of black and white at some set distances and become discernible again at a greater distance. Moreover, these earlier headsets would show artefacts caused by viewer movement and temporal changes.

Similarly, in COTSVR, [39] evaluated commercial off-the-shelf virtual reality devices (Oculus Rift and HTC Vive) based on their compatibility with specific military

applications. The authors simulated a Snellen chart directly in front of the user at a fixed distance of 20 feet. The chart was scaled so that the topmost "E" was 88.6mm tall. They report a single user in their study. The subject had normal vision (20/20) which deteriorated to 20/40 in the Oculus and 20/50 in the Vive. Considering COTSVR devices have a significantly higher pixel density (9.81 ppd) than the VEPAB system (4.05 ppd), it is expected that they report a higher acuity than VEPAB. However, COTSVR results stand in stark contrast with the average acuity of 20/100, reported by [40], who used a HTC Vive Pro (13.09 ppd). In 3DSVA, these authors conducted a more controlled experiment, where they ensured that the real and virtual test environments were as similar as possible. The participants were tested in a room with a real Snellen visual acuity chart. Next, a 3D scan of the room was used to create a virtual test where the visual acuity chart was rendered in the exact same place as its real-world counterpart. This setup ensured that the placement of the chart, the illumination and dimensions of the room were not going to influence the outcome of the experiment.

All of the previous tests have simply adopted the physical visual acuity tests into the virtual space. However, the next few tests have designed VA tests that leverage the advantages of a controllable simulation. For example, in VAVR [41] Landolt C optotypes of 8 different orientations were projected to the center of the subjects field of view, one at a time. When, more than half of the randomly oriented C of the same size are recognized correctly, the size is decreased. This continues until the case where more than half of the orientations are misidentified. The size is then set to $l = \frac{l_{wrong} + l_{correct}}{2}$. Such resizing continues until a threshold is reached. The authors report a VA collapse from (20/15 - 20/10) range to (20/35-20/25), clearly displaying significant improvement over the previously reported methods. In ARVA [42], the authors proposed a similar approach to VAVR, where an automated system would

go through three phases to assess the VA of the subject. However, the authors used augmented reality glasses that had significantly higher pixel density (31.6 ppd) than virtual reality glasses, due to their small field of view. ARVA was used to measure the acuity of 53 subjects, and resulted in acuity disagreement of .05 logMAR between automated AR and manual measurements. Their 3 phased automated approach meant that the mean test time was half as long as the manual test.

[43] assessed the dynamic visual acuity of 22 participants in a virtual environment. The user's head was rotated with a constant speed while a they were being tested with a virtual and stationary Sloan acuity chart. The authors report that dynamic VA is not affected by the low pixel density of VR displays the way static VA is. This is highly promising because, because a VR-based dynamic VA could accurately predict the driving capability of a user, more so than static VA can.

Static visual acuity is widely used whereas dynamic visual acuity is mostly limited to assessing athletes [47], despite the evidence that it is a useful marker for various daily activities such as driving, reading road signs etc. [48, 49].

3.1.2 Contrast Sensitivity in VR

Contrast sensitivity refers to a measure of how much contrast a person requires to see a target. Like VA, CS is examined through charts with test targets that are either sine-wave gratings or letters. Pelli-Robson CS is a letter chart, which is simple, quick and provides significantly more repeatable measures than sine-wave grating charts such as the Vistech25, FACT25, or CSV-1000 charts [50]. Abnormal contrast sensitivity is a sign of optic nerve dysfunction. Some patients with optic neuropathy have good acuity but may have reduced contrast sensitivity thresholds. It is also helpful in patients with congenital dyschromatopsia. A decrease in the contrast sensitivity function can lead to a loss of spatial awareness and mobility as well as an increase in the risk

of accidents. Contrast sensitivity may also affect the ability to: walk down steps, recognize faces, drive at night or in the rain, find a telephone number in a directory, read instructions [51].

In 3DSVA [40], the subjects were virtually 3m away from contrast discs of 7mm diameter, which had two spatial frequencies, six contrast levels and three orientations. The authors record the lowest contrast circle that the observer is able to correctly identify the orientation of. The preliminary results show that the subjects performed worse in the virtual CS test as well. The suboptimal resolution of the VR display was likely responsible for this poor result.

3.1.3 Metamorphopsia in VR

The Amsler Grid is an alternative to central VF analysis if a quick assessment of macular function is required, and it is particularly useful in cases with metamorphopsia or visual distortion. It is a grid of horizontal and vertical lines used to visualize the distorted perception of individuals. This test is generally administered using a paper. The 3-D Computer-Automated Threshold Amsler Grid Test [x] is a less subjective, more robust variation of the paper-based perceptual test. 3D Amsler grid is performed on a laptop computer with a touch sensitive screen that takes about five minutes per eye to complete. With one eye covered, a person sits in front of a computer screen divided into a grid. The subject stares at a central spot on the touch-sensitive screen and, using a finger, outlines missing areas of the grid. The same procedure is then repeated at various greyscale levels - simulating increasing degrees of contrast - and the respective results are recorded and later automatically displayed by the computerized test program.

In [44], the authors proposed a parameterized model to assess and simulate metamorphopsia. Their model uses the Amsler grid to measure neuro-ocular damage in

the form of luminance degradation, rotational distortion and spatial distortion. The authors propose to use this simulated model of individual perception to predict and track disease progression. In [45], the authors conducted a small preliminary study with healthy participants, presenting them with already simulated perceptual loss in one eye. The participants then had to adjust parameters of the model to replicate the distortion in the other eye. Such a method is very helpful in communicating specific perceptual loss to physicians and would greatly aid in designing specific compensation.

3.2 Simulating Vision Impairments in VR

Day-to-day quality of life is tied to activity limitation and independence. Virtual Reality can facilitate wider reach and impact by providing a safe, cheap, interactive and supportive platform. We are going to consider three aspects of communicating insights about visual disorders. First, creating awareness among the general population who have limited knowledge, or even misconceptions about VI.

Consider raising awareness about the various manifestations of vision loss and their causes. It is one of the important objectives of these non-profit organizations. VAMR can

Ocular diseases are diverse in the way they manifest in a patient's vision. For example, cataracts occur due to opacification of the natural crystalline lens. This clouding of the lens present with blurry, dim, or even altered color vision. Patients with serious cataract progression often cannot recognize faces. This presents as a serious detriment to the quality of life, such as meeting new family members like grandchildren but not being able to identify their face. Severe cataracts can also limit independent transportation options such as driving a vehicle or riding a bike, significantly limiting freedom and quality of life. While cataracts severely diminish

the quality of life, other ocular symptoms that present differently but have similar results. Severe AMD, which affects the retina, often presents with significant loss of central vision and vision distortion, often leading to the inability to drive or recognize individuals. In a survey on public perception of vision loss, "loss of independence" was ranked as the second most concerning consequence of vision loss with "quality of life" as the top concern [52]. The definition of legally blind is visual acuity in one eye of 20/200 or worse [53]. Both cataracts and AMD can cause one to be legally blind but affect completely different parts of the eye and present completely differently. In the vision loss survey, 25% of individuals were unaware of any eye conditions [52]. While blindness is one of the most feared conditions, aspects regarding eye health such as important eye diseases and behavioral/hereditary risk are not well known to the public. The lack of awareness about these eye conditions [54–58] are a key driver behind the high rates of late diagnosis [59]. Campaigns seeking to increase awareness on the importance of regular eye examinations and eye care services have been shown to be effective among older populations and those with diabetes [60,61]. VR can supplement to the success of these campaigns and increase public awareness of eye conditions and risk factors. Basic simulations would help participants recognize precursors of various eye conditions in themselves and others, allowing them to seek professional help before a disease can reach a debilitating stage. By integrating more engaging and realistic experiences of different types of eye conditions into campaigns, the public may develop a deeper insight into the serious consequences for the affected individuals. Accurate simulation of patients' perception would help physicians better understand and address the needs of their patients [62]. Clinicians can use these simulations to design and administer care that is more personal to the patient.

The earlier technologies relevant to this section are primarily concerned with giving a rudimentary idea about the perceptual difficulties faced by patients of the more

prevalent conditions such as cataracts, glaucoma and AMD. The later studies focus on a wider array of conditions such as DR, color deficit, double vision, among others. These studies also use photo-realistic environments, high-fidelity impairments to accurately portray the actual perception of individual people. We can also see the tendency to use AR more in the later studies as commercial HMDs are equipped with more capable stereocameras and eye-tracking.

In 2002 [63] demonstrated that letting caregivers experience the perceptual effects of stroke influenced their empathy and understanding of patients' daily difficulties. In addition to restricting the view of the participants' left hand side, the authors simulated nausea and dizziness through motion blur and camera movement. As a result, healthy participants reacted like a typical stroke patient, reinforcing the efficacy of VR as an educational tool that can be utilized in a wide array of settings.

In 2006, a similar tool was developed by [64] for patient education and healthcare practitioner training but for common eye conditions instead of stroke. The authors use a drafting table format VR display to simulate impaired sight caused by glaucoma, AMD, protanopia and DR. However, the VR system was neither portable nor affordable, making it unsuitable as a learning tool.

In 2016, [65] developed a portable and inexpensive system that simulated the effects of eight common eye pathologies. The authors use a single camera to create a video see-through system that uses image processing to black out the scotomatous regions. For a better, stereoscopic simulation, [66] used two cameras to simulate cataracts, glaucoma, and lower latency due to natural aging. [67] developed a VR simulation that can effectively communicate the sensation of oscillopsia. However, none of these techniques offer user calibration, which enforces that there is considerable variation in the impairment caused by most diseases. People exposed to these variations will not misjudge an individual's capabilities based solely on common man-

ifestations. Researchers have shown that people with VIs can perform a wide range of tasks with assistive technology [68–72]. Yet the employment rate for visually impaired people is still very low. Misconceptions regarding the disabling nature or generalization of various diseases are the leading cause of this phenomenon [73]. Raising public awareness regarding the manifestation, variety and characteristics of these eye diseases can therefore help curtail this practice. Sight-enhancing medical devices, such as bioptic telescope glasses, in certain states allow for visually impaired drivers to drive on the road [74]. A 2020 study demonstrated that there was no statistical significance in low-vision individuals with bioptic telescope glasses being more prone to near-collision accidents compared to regular drivers [75].

[76] address this issue by integrating eye-tracking and symptom adjustment. Their work overcomes one of the limitations of previous simulations where central vision loss was central to the screen instead of the users' gaze. Now, irrespective of the user's head position the scotoma will move along with their line of sight. The system proposed by [77] is able to display the progression of vision diseases using multiple ophthalmic assessments. Their monocular and binocular modes enable patients and their relatives to better comprehend the severity and progression of a vision disease. In monocular mode, the visual field of the worse eye can be examined with the better performing one. [78] shows a medically informed AR/VR simulation of AMD, refractive errors and cataract that has eye-tracking, stereoscopic video see-through and user calibration.

Recently, as part of a federal effort to disseminate accurate eye health information, the National Eye Institute (NEI) has launched a smartphone VR app [79] to simulate common eye diseases, including AMD, cataracts, glaucoma, and DR. Even though this application can't be tweaked to simulate vision loss of individuals, it can serve as a pioneering tool to inform the public about these ocular diseases.

Chapter 4

Methodology

4.1 Pipeline for Measuring Visual Acuity

4.1.1 Far Visual Acuity

Our VA test is structured slightly different from standard chart based VA measured by eye clinicians. Instead of displaying a whole eye chart, our test presents one symbol at a time. Standardized landolt C character was chosen as the presentation optotype because it allows users to identify the direction of the gap and therefore the process can be simplified. However, if a letter acuity optotype characters were shown instead, the patient would need to look at the keyboard to respond. The primary goal of this test is to measure the VA of each eye separately and then binocularly. The following test protocol provides a detailed description on how we designed this test:

At the start of the monocular assessment protocol, only the eye being tested can see a photopic background. We use emissive material in unreal engine to set the luminance of the background to 200 cd/m^2 . The other eye is shown a completely dark scene where the luminance is set to 0. Landolt C optotype materials were custom

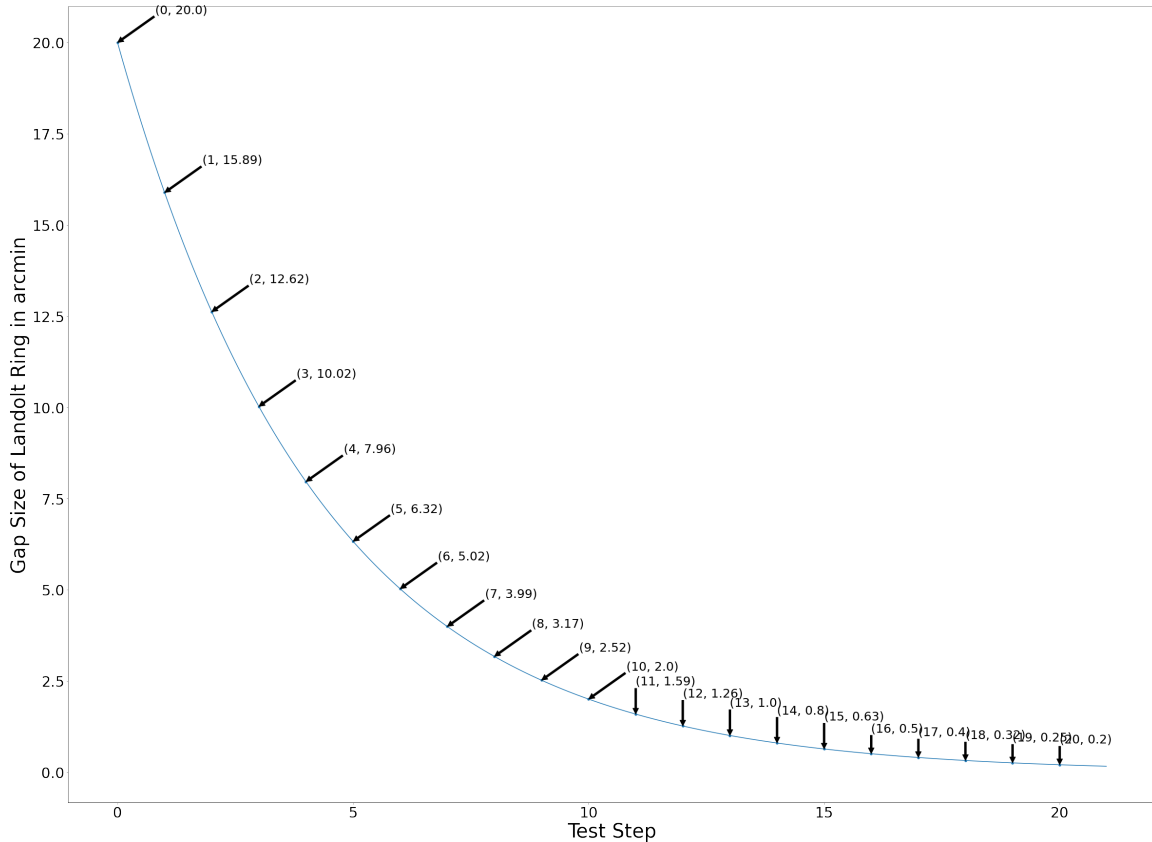


Figure 4.1: Continuous sampling of Gap size from curve

made so that they could be stretched and shrunk indefinitely without causing any visible distortions. This also allowed us to set the optotype brightness so that it was within the required luminance range (30 cd/m^2).

For both the monocular and binocular tests, we use place the landolt rings at a distance of 3 metres from the observer. At the start of every test, the Landolt C is projected at the centre of the screen, with its gap at 1 of 8 possible positions [Figure 2.2\(b\)](#). The 8 possible directions are: up, down, right, left and diagonal positions in between. The gap directions are chosen randomly, however, the gaps are never generated at the same orientations consecutively. The participants indicate the orientation of the gap by using the numpad keys. We choose this approach instead of the motion controller because it is more reliable and less prone to accidental clicks.

In a standard eyesight test it is recommended that the viewers read fewer (3 times) of the largest optotypes compared to the smaller ones (typically 5 times). However, we show the same sized characters five times no matter the dimensions. Our VR environment can hold considerably bigger optotypes because they are shown one at a time. More than 50% of the Landolt rings have to be identified correctly, for the trial to be considered passed. If passed, the Landolt ring will decrease logarithmically. However, if the viewer fails, then the optotype size is increased.

The stimulus size is changed based on the function depicted in [Figure 4.1](#). It depicts a monotonically decreasing function where the later trials have less size difference. In our preliminary trials we used the following equation to determine the appropriate next size:

$$trial_{current} = \frac{trial_{correct} + trial_{incorrect}}{2} \quad (4.1)$$

where we start with $trial_{correct}$ and $trial_{incorrect}$ values initialized to zero.

$$gap_{current} = \frac{20}{10^{\left(\frac{trial_{current}}{10}\right)}} \quad (4.2)$$

This method ensured that the angular difference between consecutive stimuli were small but perceivable. This is because most human sensory functions follow a logarithmic function.

This $gap_{current}$ was in arc minutes. In order to get the actual dimension of the presentations necessary at a distance of 3m, we used the following [Equation 2.2](#), with the $f = 300$:

$$d = 300 \times \tan\left(\frac{gap_{current}}{12}\right) \quad (4.3)$$

After 3 (if all presentations are correctly identified) or 5 optotypes (if all pre-

sentations are misidentified) the assessment proceeds to the next trial following the Equation 4.4:

$$trial_{correct} = \begin{cases} trial_{current} & \text{if at least 50\% of } gap_{current} \text{ optotypes are perceived} \\ trial_{correct} & \text{otherwise} \end{cases} \quad (4.4)$$

$$trial_{incorrect} = \begin{cases} trial_{current} & \text{if at least 50\% of } gap_{current} \text{ optotypes are missed} \\ trial_{incorrect} + 2 & \text{no incorrect trials so far} \\ trial_{incorrect} & \text{otherwise} \end{cases} \quad (4.5)$$

What	Decimal acuity	Snellen Ratio (ft)	Snellen Ratio (m)	LogMAR
<i>Shorthand</i>	VA_{dec}	$VA_{Snellen}$	$VA_{Snellen}$	VA_{LogMAR}
<i>Formula</i>	$1 / MAR$	$20 / (20 \cdot MAR)$	$6 / (6 \cdot MAR)$	$\log_{10}(MAR)$
<i>“normal”</i>	1.0	20/20	6/6	0.0
<i>“low”</i>	0.1	20/200	6/60	1.0
<i>Conversion</i>	$10^{(-VA_{LogMAR})}$	$VA_{Snellen} \equiv VA_{dec}$	$VA_{Snellen} \equiv VA_{dec}$	$-\log_{10}(VA_{dec})$

Figure 4.2: Conversion between different types of VA measures [1]

Different stimuli are continually presented until the difference between successive optotypes go below a threshold. When the threshold is reached, the value of the current gap in the landolt ring is used to compute the minimum angle of resolution

(MAR) for the participant. Next, the visual acuity is reported in logMAR. Other units can also be selected, We used [Figure 4.2](#) to convert the logMAAR value to the other units.

Monocular and binocular tests have different locations of presentation, according to the eye tracking data in the calibration phase. Low vision VA can also be measured with our system, where optotype sizes are presented according to the chart [Figure 4.3](#).

Measure	Finger counting (at 30 cm)	Hand movement	Light perception	No light perception
<i>Shorthand</i>	CF	HM	LP	NLP
<i>Suggested value</i>	1.9 LogMAR	2.3 LogMAR	(2.7 LogMAR)	(3.0 LogMAR)

Figure 4.3: Low vision Acuity equivalent [1]

4.1.2 Measuring Dynamic VA

Dynamic visual acuity is measured using the same optotypes as Distant VA. The optotype starts at 20° temporal from the central visual field and continues to move back and forth in the horizontal plane in a 40° arc (20° side to side to side) at 2 Hz (exceeding compensation by the pursuit system). The subject tries to recognize the direction of the gap similar to the static test. We only test the dynamic VA binocularly. For our tests, the moving stimuli were set to a constant linear speed of 1 meter per second.

Luminance _{Target}	Lumance _{Surround}	Contrast _{Michelson}	Contrast _{Weber}	logCS _{Weber}	ContrastRatio	C _{Aulhorn}
99,9 cd/m ²	100 cd/m ²	0,050 %	0,1 %	3,00	1,001	
99,01 cd/m ²	100 cd/m ²	0,50 %	1,0 %	2,00	1,010	
97,56 cd/m ²	100 cd/m ²	1,235 %	2,4 %	1,61	1,025	
95,24 cd/m ²	100 cd/m ²	2,44 %	4,8 %	1,32	1,05	
87,72 cd/m ²	100 cd/m ²	6,54 %	12,3 %	0,91	1,14	1 : 1,14
80 cd/m ²	100 cd/m ²	11,1 %	20,0 %	0,70	1,25	1 : 1,25
68,03 cd/m ²	100 cd/m ²	19,0 %	32,0 %	0,50	1,47	1 : 1,47
59,88 cd/m ²	100 cd/m ²	25,1 %	40,1 %	0,40	1,67	1 : 1,67
50 cd/m ²	100 cd/m ²	33,3 %	50,0 %	0,30	2,0	1 : 2,0
37,04 cd/m ²	100 cd/m ²	45,9 %	63,0 %	0,20	2,7	1 : 2,7
20 cd/m ²	100 cd/m ²	66,7 %	80,0 %	0,10	5,0	1 : 5,0
4,35 cd/m ²	100 cd/m ²	91,7 %	95,7 %	0,02	23	1 : 23
1 cd/m ²	100 cd/m ²	98,0 %	99,0 %	0,004	100	
0,1 cd/m ²	100 cd/m ²	99,8 %	99,9 %	0,0004	1000	

Figure 4.4: Conversion between contrast sensitivity metrics [1]

4.2 Pipeline for Measuring Contrast Sensitivity

In the background section we discussed how CSF can be measured by varying both contrast and spatial frequencies. However, measuring the whole contrast sensitivity function can take upto 40 minutes. In our current set of visual assessment tests we have implemented an adaptation of the shorter Pelli-Robson contrast test. Gabor patches Equation 2.4 are a better alternative to landolt rings for such tests because the spatial frequencies can be varied without decreasing the size of the stimuli. Moreover, compared to letter stimuli, subjects do not need to look at the keyboard to correctly respond to the direction of the gabor patch. Like the landolt ring, we also created unreal materials based on gabor patches so that they can be infinitely stretched or shrunk without distortions. The following equation was used for that purpose:

$$L(x, y) = L_0 \{ 1.0 + c \times \sin[2\pi f(x \cos \theta + y \sin \theta)] \times e^{-(x^2+y^2)/2\sigma^2} \} \quad (4.6)$$

Unlike the VA procedure, our contrast sensitivity test is not adaptive to user response. Gabor patch stimuli were presented within 11 possible grating spatial frequencies which were spaced log linearly from 0.6 to 20 cpd; the 46 possible grating contrasts were spaced log linearly from 0.15% to 99%. According to the Equation 4.6 where c is the signal contrast, $\sigma = 1.87$ deg is the standard deviation of the Gaussian window (which was constant across spatial frequencies), and the background luminance L_0 was set in the middle of the dynamic range of the display ($L_{min} = 3.1cd/m^2$; $L_{max} = 120cd/m^2$). The stimulus orientations would be in one of 4 different directions.

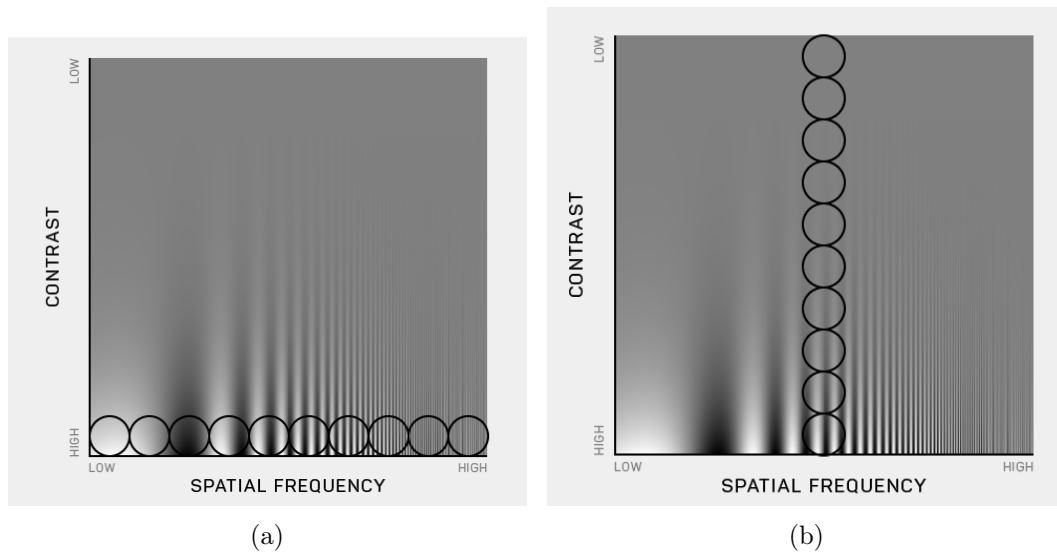


Figure 4.5: Changing stimuli spatial frequency and contrast

The test starts off with a michelson contrast 99% which is a very high contrast. The size of the patch was fixed at a visual angle of 12° . If the orientation was correctly detected at least half of the time (with 5 maximum presentations per contrast level), then the contrast value was decreased log linearly as described earlier. If the subject fails to correctly identify at least half of the presentations, then the test is terminated and the contrast level is reported in logCS based on the following conversion between michelson contrast and logCS:

$$\log CS = -\log_{10} \frac{2 \times \text{Contrast}_{michelson}}{1 + \text{Contrast}_{michelson}} \quad (4.7)$$

This logCS value can then be reported in weber units:

$$\text{Contrast}_{weber} = 100 \times 10^{-\log CS} \quad (4.8)$$

4.3 Simulating Age-related Macular Degeneration

We parameterize the perceptual impairment and vision deficit in different AMD types based on localized physiological damage. We will utilize the locus of the perceptual loss to create parametric models for the visual deficit. This will enable a central vision loss simulator for a variety of impairments associated with AMD.

4.3.1 Modeling Perceptual Deficit

Our parametric model for the perceptual loss is a 4-tuple of the following form

$$\mathcal{P} = (\Gamma, \Omega_\lambda, \mathbf{R}_\theta, \Psi) \quad (4.9)$$

where Γ represents luminance degradation, Ω_λ represents the visual field loss region with λ as the cut-off degradation determining the boundaries of the scotoma, \mathbf{R}_θ is the rotational distortion matrix within Ω_λ , and Ψ is the a Sinusoidal mapping function representing the spatial distortion.

Modeling Luminance Degradation Effects

A Gaussian Mixture Model (GMM) was used to represent the degradation in luminance caused as a result of damage to the cone photoreceptors. Therefore, luminance

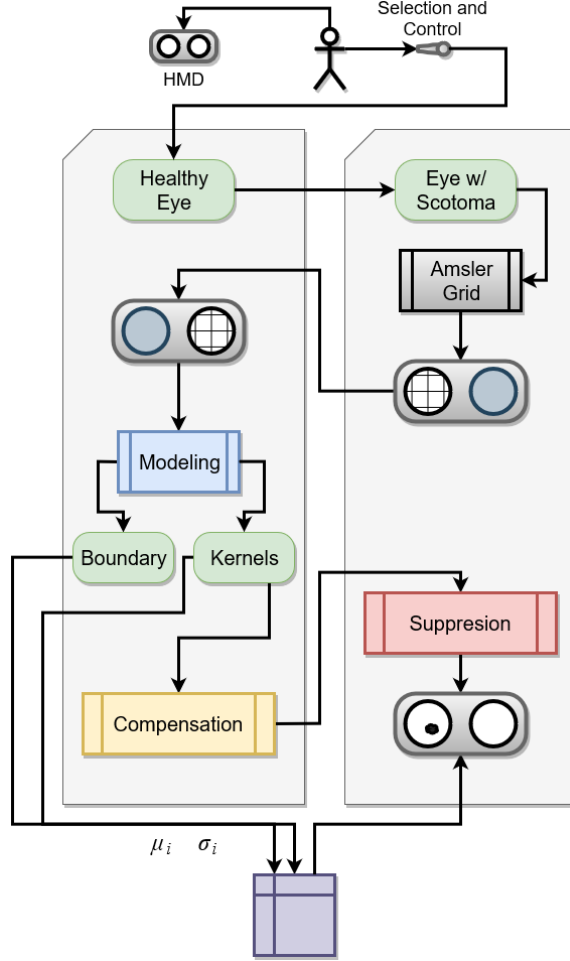


Figure 4.6: Simulating perceptual deficit

degradation, Γ takes the following form:

$$\Gamma = \sum_{i=1}^N \omega_i \mathcal{N}_{\vec{\mu}_i, \sigma_i}(u, v) \quad (4.10)$$

where u and v are the coordinate locations on the 2-D visual field, N is the number of Gaussian kernels (Normal distributions) modeling the deficit in the luminance perception in the visual field, and ω_i is the amount of luminance deficit caused by each Gaussian kernel. $\mathcal{N}_{\vec{\mu}_i, \sigma_i}(\cdot)$, are the gaussian kernels where $\vec{\mu}_i = [\mu_i^u, \mu_i^v]$ represents the center and σ represents the standard deviation of the distribution.

Figure 4.7 shows how a single illumination degradation kernel ($N = 1$) affects

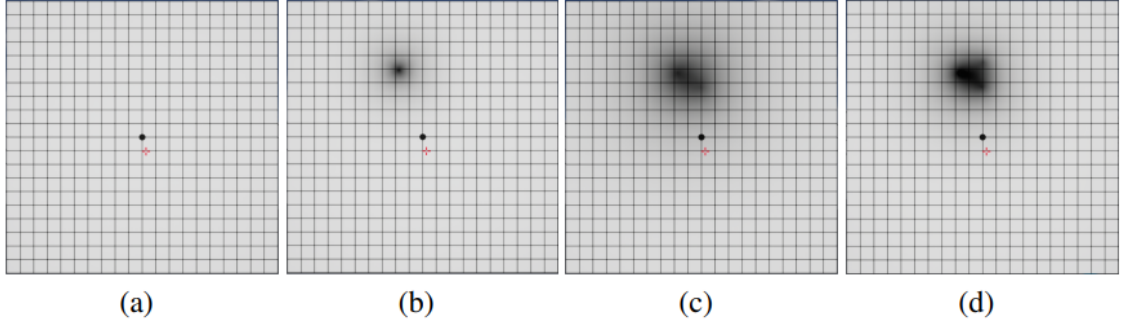


Figure 4.7: Illumination Degradation Γ , represented by the proposed parametric model

an Amsler grid. A significant advantage of the proposed parametric model is in its ability to represent complex illumination degradations caused by the progressive retina damage. With disease progression there may be additional areas of damage surrounding the earlier scotoma, which can be modeled with multiple such kernels ($N > 1$). Note that for each Gaussian kernel, the luminance deficit is the highest at the centre and diminishes with distance. ($\vec{\mu}$).

Modeling Perceptual Deficit Region

Once the luminance degradation model is established we identify the region in the visual field in which the perceptual impact is significant [Figure 4.8](#). Let's call this region Γ . Setting a cutoff value $0 < \lambda < 1$, the region Ω can be determined as the following:

$$\Omega = \{(u, v) \in \mathbb{R}_{[0,1]}^2 \mid \Gamma(u, v) \leq \lambda\} \quad (4.11)$$

The solid blue area in [Figure 4.8](#) shows the perceptual deficit region Ω for the modelled illumination degradation of [Figure 4.8](#). Note that since λ is a free parameter, it can control the boundary of the perceptual deficit region Ω . The larger the value of λ , the broader the regions Ω will be. We can also visualize multiple regions with

different prominent levels of illumination degradation [Figure 4.9](#).

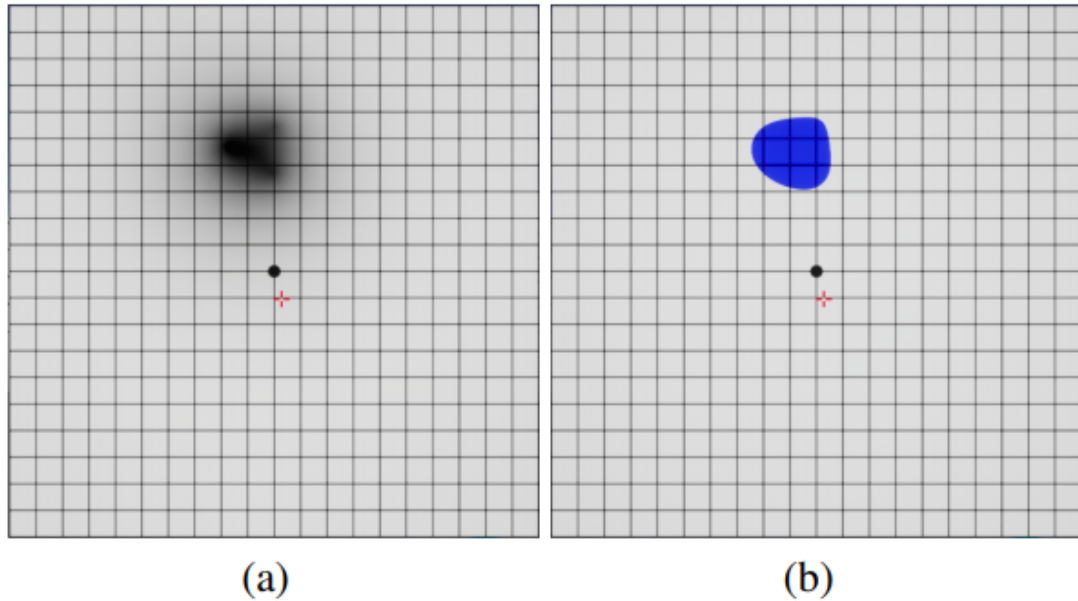


Figure 4.8: Perceptual deficit region Ω , represented by the proposed parametric model. The area within the solid blue region represents illumination degradation of more than λ percent.

Modeling Rotational Distortion

With the position and extent of the perceptual damage determined by the centers ($\vec{\mu}_i$) of each Gaussian distribution in [Equation 4.10](#), we can model the rotational distortion as a result of physiological damage. Rotational distortion, R_θ , is one of the components of the perceptual loss model, \mathcal{P} [Equation 4.9](#). Let θ be the angle of rotation, each point in the visual field will be rotated by the following rotation matrix:

$$\mathcal{R}'_\theta = \begin{bmatrix} \cos \theta & -\sin \theta \\ \sin \theta & \cos \theta \end{bmatrix} \quad (4.12)$$

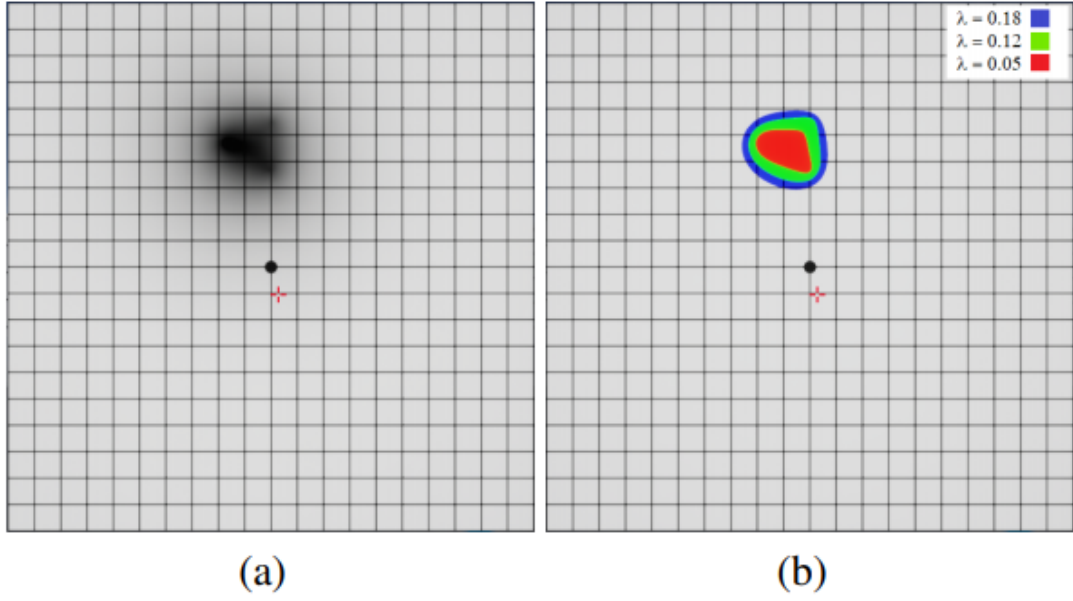


Figure 4.9: Different perceptual deficit region Ω at different boundary strength λ . The area within the solid blue, green, and red regions represents decreasing boundary strength of $\lambda = 18\%$, $\lambda = 12\%$, and $\lambda = 5\%$, respectively.

Since the perceptual impact decreases as we get farther away from the central location of the scotoma, distortion too becomes less and less prominent. Therefore, we model the rotational distortion within the damaged region Ω for each of the Gaussian kernels as:

$$\mathcal{R}_\theta = \sum_{i=1}^N \omega_i \mathcal{N}_{\vec{\mu}_i, \sigma_i}(u, v) * \mathcal{R}'_\theta \quad (4.13)$$

The effects of this rotational distortion within the affected region of the visual field is shown in [Figure 4.10\(a\)](#). In [Figure 4.10\(b\)](#) the model utilizes a single Gaussian kernel with its impact region depicted in [Figure 4.10](#) at $\lambda = 0.5$. A rotation of $\theta = \pi/2$ will cause the rotational distortion shown in [Figure 4.10\(c\)](#). The combined effects of the luminance loss and rotational distortion can be observed in [Figure 4.10\(d\)](#).

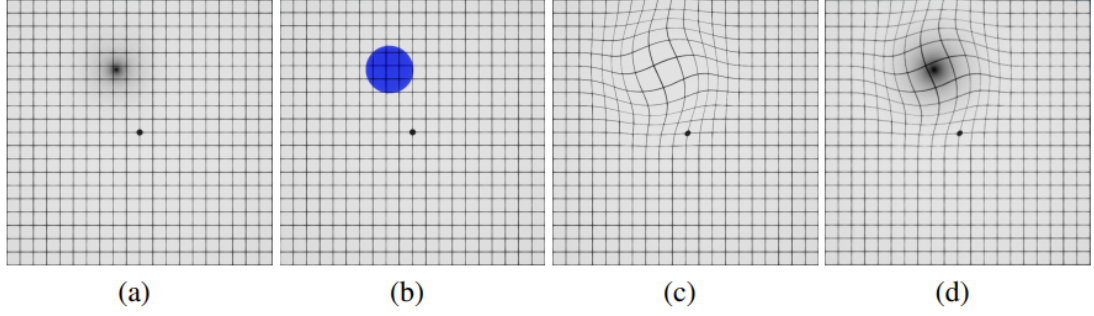


Figure 4.10: Modeling rotational distortion: (a) A single Gaussian kernel illumination degradation. (b) The perceptual impact regions with $\lambda = 0.5$. (c) the Rotational distortion with $\pi/2$ angle. (d) Both illumination degradation and rotational distortion.

Modeling Spatial Distortion

Finally the spatial distortion component Ψ is incorporated. Ψ represents the spatial shift perceived by the patient as a result of the damage to the retina that is not captured by the rotational distortion model described earlier. Imagine the fabric of the retinal layer being stretched or squeezed onto the deficit region. A vector field dictates the spatial translation of points within the visual field. The complete spatial distortion vector field Ψ is defined as:

$$\Psi = \sum_{i=1}^N \mathcal{N}_{\vec{\mu}_i, \sigma_i}^i(u, v) * \mathbf{I}_2 * \begin{bmatrix} u - \mu_u^i \\ v - \mu_v^i \end{bmatrix} \quad (4.14)$$

where \mathcal{N}_i represents each of the Gaussian deficit models with $\vec{\mu}_i$ mean and σ_i standard deviation. \mathbf{I}_2 represents the 2×2 identity matrix, and u, v are coordinates within the visual field. To illustrate this spatial distortion effect, suppose we have a single scotoma at the central location of the visual field (i.e., $[uv]^T = 0$). The vector field representing the spatial distortion model will be of the following form (depicted in [Figure 4.11](#)):

$$\Psi \approx \begin{bmatrix} e^{-\frac{(u-\mu_u)^2+(v-\mu_v)^2}{2\sigma^2}} * (u - \mu_u) \\ e^{-\frac{(u-\mu_u)^2+(v-\mu_v)^2}{2\sigma^2}} * (v - \mu_v) \end{bmatrix} \quad (4.15)$$

Figure 4.11 shows the vector fields that denote the stretching of the visual field as a result of the physiological damage. A single Gaussian kernel will generate a simple vector field shown in Figure 4.11(a), while a more complex spatial distortion will require a Gaussian Mixture Model as seen in Figure 4.11(b).

The strength the spatial distortions can be varied as depicted in Figure 4.12. At the early stages of the disease a single Gaussian kernel may be sufficient to model the distortions Figure 4.12(a), but as the disease progresses more complex models will be required. The proposed mixture model shows the flexibility to represent the distortion changes as the disease progresses without the need to fundamentally change the model, but rather increase the number of Gaussian kernels Figure 4.12(b-c).

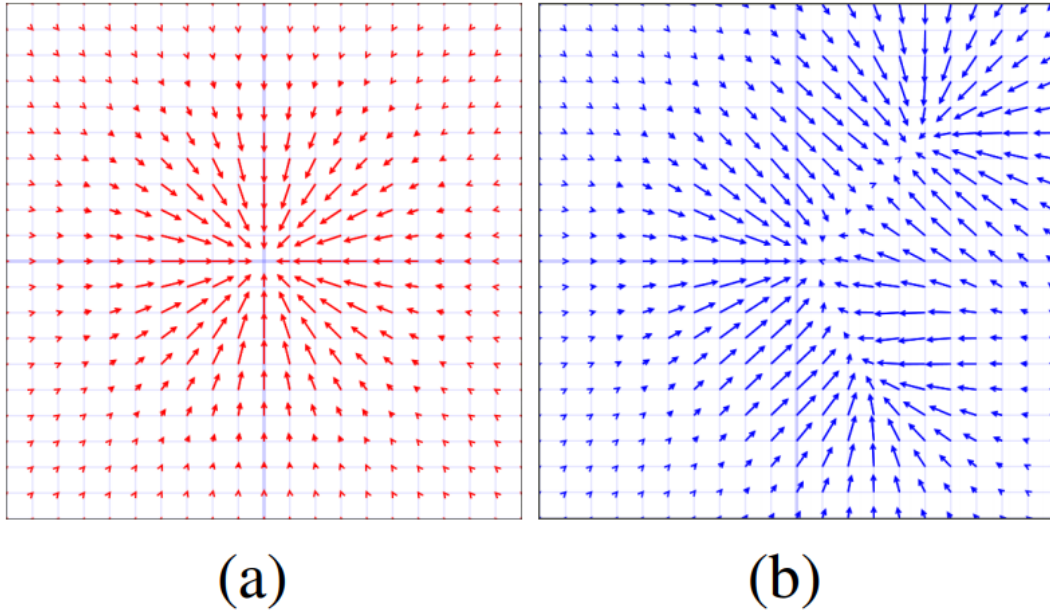


Figure 4.11: : Vector fields representing the spatial distortion maps, as modeled by: (a) a single Gaussian kernel, and (b) multiple Gaussian kernel

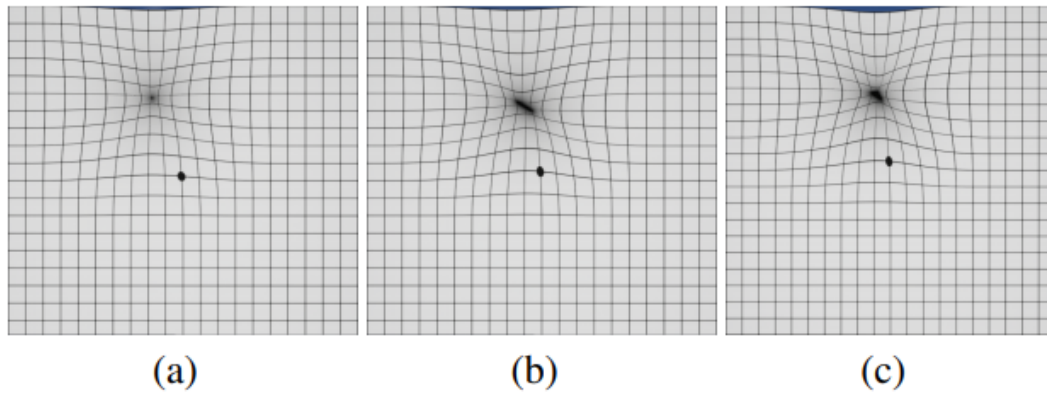


Figure 4.12: Spatial distortion of the Amsler grid as represented by the Ψ component of the proposed model. Note the model adaptation and its ability to capture disease progression: modeling spatial distortion with (a) a single Gaussian kernel, (b) two Gaussian kernels, and (c) three Gaussian kernels.

4.3.2 Modeling Scotoma Suppression

After we configure and simulate the perceptual deficit in the healthy eye, inverse of the parametric model is applied to compensate for the simulated perceptual deficit. This compensation is then applied to the eye with the scotoma. This will recover some functional vision.

HTC Vive developed an Unreal Engine Plugin called SRanipal that allows for development of eye-tracked Virtual Simulation for the Vive Headset. We use it to track the gaze of the user in a simulation and then suppress the distortions on the affected eye. Unreal Engine allows for dynamic material rendering which can be applied to the two eyes separately. As the subjects moves their gaze across the simulation, the suppression moves along with the gaze. This way the healthy eye can fill in the distorted area, replacing distortions created by the scotomatous eye. In future works, we plan to create a reverse effect that can compensate the distortion completely without the need of suppression.

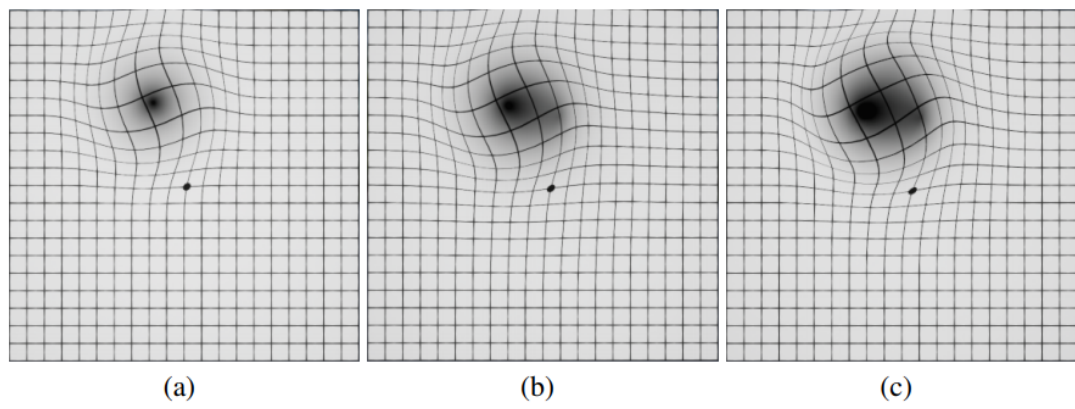


Figure 4.13: Rotational distortion and illumination degradation as the disease progresses.

Chapter 5

Experiments

5.1 Technology



Figure 5.1: HTC Vive Pro Eye System

We used Epic’s game engine UnrealEngine 4(UE4), version 4.24 for this work. Like many other game engines, UE4 supports the development of VR-projects and therefore, the use of an HMD. Blueprints Visual Scripting was chosen as scripting system, which is characterized by the employment of a node-based interface in order to create gameplay elements. Only the results of the user study were recorded with the use of a C++ file. We used the HTC VIVE Pro Eye headset shown in [Figure 5.1](#), which is supported by SteamVR, a tool for experiencing VR content. The HTC VIVE Pro Eye headset features a display with a resolution of 2880 x 1600 (1440 x 1600 per eye) and a refresh rate of 90 Hz. The value of the pixel density is equivalent to 615 PPI (pixels per inch) per eye, while 110°(diagonal) represents the FOV. The desktop version of the project was tested on a 23“ full HD monitor connected to a PC with Intel Core-i7 8700, an Nvidia RTX 2080 GPU, and 32GB RAM.

5.2 Device Calibration

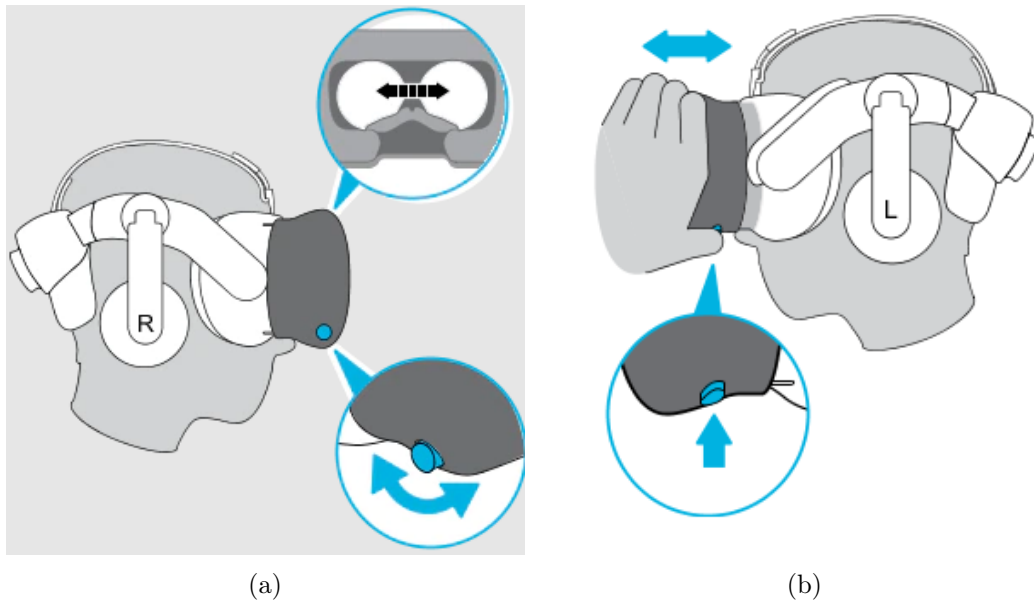


Figure 5.2: Calibration of the Headset(a) Interpupillary distance (b) Lenses

Each VR device may be setup slightly differently and the current configuration may not be optimal for each user. If the devices aren't calibrated properly, the visual assessment results may be drastically affected. To mitigate this problem, we start the VR environment and help the participants wear the headset. The headset is adjusted so that the participants are comfortable with the fit. Text is displayed in the VR environment to help participants focus by adjusting the interpupillary distance and the lens distance. The values of these adjustments are noted for each participant per trial.

5.2.1 Eye Tracking Calibration

Dynamic visual acuity and metamorphopsia use eye tracking to maintain participant fixation. When a participant's gaze deviates significantly from the recent location of the fixation, the Amsler grid is shifted to the current fixation location. In dynamic VA testing if the gaze wanders away from the stimuli, that response is discarded. In order for these measurements to work sufficiently well, the gaze tracking reliability is measured under normal circumstances. Vive Pro Eye has a plugin called SRanipal for unreal engine. We use this plugin and a checkerboard test to gauge how accurate the eye tracking works for the participant. If eye tracking data is not reliable, we do not use it in the tests.

5.3 Visual Acuity with VR

We used Freiburg visual acuity (FrACT) test [80] to compare the results of each of the static VA tests. The FrACT test was conducted at a distance of 60cm from the screen and with Landolt ring optotypes. FrACT test gave the subject a logMAR value of -0.3 [Table 5.1](#). The result was unchanged when the subject retook the test two more

times. However, the VR based binocular visual acuity gave a result of $0.625\log\text{MAR}$. That means, a person with a VA of 20/10 would only be able to exhibit a VA of 20/85 inside the VR environment. When trying to recognize the smaller optotypes, the subject reported that the display pixels could be noticed and the optotypes were too small to be represented by those limited number of pixels. These results are comparable to those obtained by [40]. Although they report that the mean acuity of 20/25 dropped to about 20/100, in our case the drop was from 20/10 to 20/85.

For monocular visual acuity, the FrACT results remained the same [Table 5.1](#). However, in the VR counterpart, the visual acuity of the right eye was measured to be $0.675\log\text{MAR}$, or 20/95.

FrACT does not have a way to measure dynamic visual acuity. In VR, the subject exhibited a dynamic VA of $0.975\log\text{MAR}$ [Table 5.1](#). However, the moving stimuli was highly inconsistent during presentation. The entire character would often disappear and reappear, with some corners getting brighter or darker. This is to be expected, because OLED displays have prominent motion blur. So, a better strategy would need to be devised to better test dynamic visual acuity.

Table 5.1: VA result ($\log\text{MAR}$) comparison

	VA Test	FrACT	VR
1	Binocular VA	-0.3	0.625
2	Left Monocular VA	-0.3	0.625
3	Right Monocular VA	-0.3	0.675
4	Dynamic VA		0.975

5.4 Contrast Sensitivity with VR

The contrast value in FrACT was measured at a distance of 60 cm. Landolt C was the optotype used in this test, compared to the gabor patch stimuli used in our VR system.

However, the measured value in both systems were very close. FrACT measured the subject’s contrast sensitivity at $1.97\log\text{CS}$, whereas the VR test measured it at $1.913\log\text{CS}$. In [40], the authors do not report the contrast sensitivity level in $\log\text{CS}$ or any other comparable metric, instead counting the number of low contrast object orientations recognized. Our test measure is a considerable improvement over their test.

5.5 Suppressing Scotoma in VR

Table 5.2: Parameters tuned to replicate the perceptual deficit caused by AMD

	Parameters	Range	Step Size
1	Mean	$\mathbf{0 \leq (\mathbf{u}, \mathbf{v}) \leq 1}$	0.1
2	Sigma	$\mathbf{0 \leq \lambda \leq 0.75}$	0.0075
3	Weight	$\mathbf{0 \leq \mathbf{w} \leq 1}$	0.02
4	Rotation	$\mathbf{-360 \leq \theta \leq 360}$	2.0
5	Distortion	$\mathbf{0 \leq \mathbf{d} \leq 100}$	7.2

The participants are first asked the demographics and computer literacy questions. The coordinator then introduces and explains the procedures for the study. After the introduction, the participants are asked to sign the study informed consent form.

The participant will first take a simple sighting alignment test to determine the dominant eye [81]. We then randomly choose to simulate perceptual deficit to either the participant’s dominant or non-dominant eye.

Then the participant is moved into the HTC Vive tracking space and was outfitted with the equipment. Once the participant is ready, both the left and right eyes are presented with the standard Amsler grid. As the participant is healthy, there should be no visible distortion in the Amsler grid. The result of distortion questionnaire were recorded as control measurements. Then a random scotoma template is simulated in

the previously chosen eye. We save the information of the distortion kernels applied to the image plane. Next, the participant answers questions related to their affected perception.

The affected area within the visual field is then suppressed in a series of steps with each step increasing the area of visual suppression. The size of the suppression increase is shown in [Figure 5.3](#).

At each stage, the participant will answer questions regarding the perceptibility of the simulated distortion. The first suppression area at which the distortion becomes imperceptible are recorded for each participant and each eye. The suppression area at which the participant start noticing that the suppression is applied are also be recorded for each participant and each eye.

Most of the experiment flows the same way for both types of participants. Instead of simulating a randomly generated scotoma, the participant tries to replicate the existing metamorphopsia into the healthy eye. After replication, the GMM kernel data is saved. Then, the simulated scotoma is removed from the healthy eye. Just like in the case of a healthy participant, the affected visual field is suppressed with a dark overlay. The size of the suppression is then gradually increased. At each stage, the coordinator asks how perceptible the distortion is as a number between 1 to 5.

At the end of the VR experiment, participants were asked to fill out a questionnaire about their experience with the simulation.

[Figure 5.3](#) shows the results of the suppression mechanism in action. Healthy participants were shown simulated scotomas, and the effects of suppression of the scotomatous region in recovering visual function were measured. It was hypothesized that once the suppression area approaches the area of scotomatous regions, the binocular interaction will allow the patient to cease to perceive the metamorphopsia in the scotomatous eye.

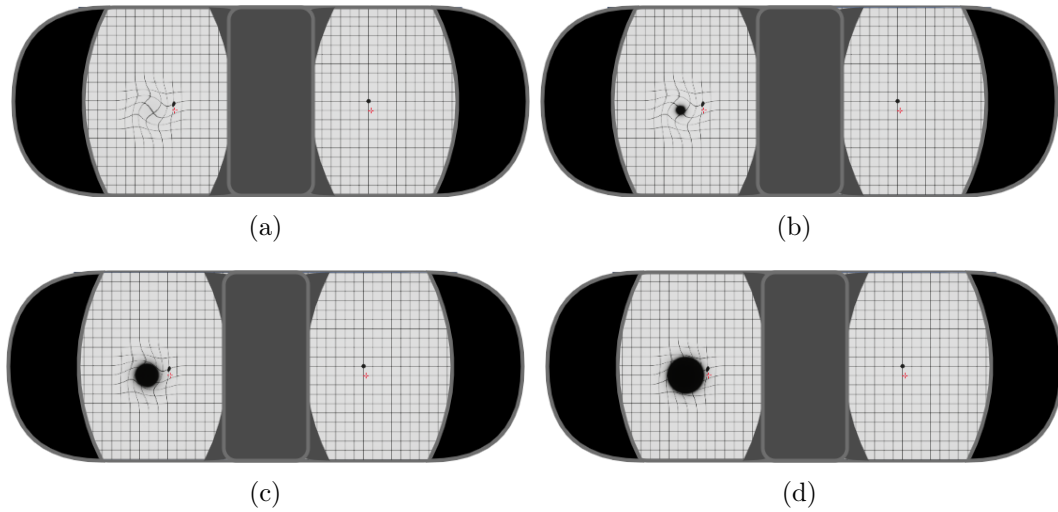


Figure 5.3: This shows what participants see when they wear the VR headset. In (a) the left eye sees an Amsler grid with simulated distortion and the right eye sees it without distortion. In (b) a small suppression is introduced to the distortion. (c) and (d) show a gradual increase in the suppression size.

Our preliminary results show that participants recovered visual function when moderate suppression levels were applied (Figure 5.3(c)) as a result of binocular interaction. We found that low suppression (Figure 5.3(b)) could not sufficiently reduce the error perception. On the other hand, the highest suppression (Figure 5.3(d)), almost the size of the scotomatous region itself, also reduced the vision function through prominence.

Chapter 6

Conclusion and Future Work

6.1 Limitations and Future Work

One of our goals was to assess the visual function from within a VR system. Our experiments showed the flexibility of our framework in supporting the combination of different distance, motion, contrast and distortions. The tests adapted to the user through pretest calibration and during-test responses, allowing us to assess a variety of different ocular functions. While the ophthalmologists we collaborate with see our assessments as a clear advancement for assessing function in a portable and affordable way, the current discrepancy between the real and virtual measures clearly need to be addressed first. One way to do this would be to create a machine learning framework that can correlate performance in the VR system to performance in the real world standardized tests. However, to create and then validate the quality of such a system, ground truth must be collected. Specifically, for SANS monitoring a large amount of terrestrial dataset would have to be collected and analyzed.

Since the characteristics and severity of AMD is hard to assess, patients who have

this eye disease are the only ones who can provide us with a useful feedback. Unfortunately, our planned study with 30 participants could not be arranged due to the COVID-19 pandemic and we are only able to present preliminary results. The few experiments we could run showed that our system results are not yet viable. We believe that these tests can be improved in future work, by working closely with ophthalmologists and patients, and that our methodology and framework can complement even more visual assessment tasks.

As discussed in [section 2.2](#), there are many functions of the ocular system that can be measured with a variety of functional tests. In this work we selected some of these tests, which we deemed to have the highest impact on perception. However, effects such as perceptual filling in are not present in this work. We chose this approach because one symptom can influence the perception of another symptom. If we, for example, do a VA test or calibrate VA with already reduced contrast, we will get a different result than when testing or calibrating VA in isolation.

We used our parametric model to simulate AMD, informed by expert knowledge from ophthalmologists and medical images. However, we have not yet been able to evaluate the accuracy of these simulations with real patients. Geographic atrophy or a loss of tissue in the macula is a common finding in medical images of dry AMD. [\[82\]](#) reason that a central vision loss does not imply perceptually black areas in the center of the field of view (like used in our simulation of AMD), since affected people may experience perceptual filling-in, a phenomenon where the brain auto completes missing information by extrapolating from the surrounding area of the scotoma.

Moreover, as we have described in the experiment section, dynamic visual acuity measure in our system is deeply affected by OLED motion blur. Static VA is highly limited by the pixel density of the head mounted displays. Our VR device only had 13ppd whereas for basic visual acuity measurement a minimum 60ppd is required.

The range of contrast that can be depicted is restricted by the limited dynamic range of VR devices. When these issues can be resolved, proper visual assessment can be possible.

6.2 Future Works

Better calibration of the VR device can improve the quality of the measurements acquired from the vision tests. For example, creating VR-based dominant eye detection, blind-spot localization, ocular alignment measurement algorithms can improve the calibration process. Moreover, using photometers we can better map unreal lighting to VR display capabilities. Calibrating the contrast test considering the maximum and minimum luminance of the HTC vive device is likely to improve the CS results. More diverse test environments such as scotopic and mesopic lighting conditions can be created to gather a more rich pool of assessment data for finding correlation with known pathologies.

The proposed system is the first, and only, system to date that allows patients suffering from neuroocular pathologies establish perceptual deficit models of their vision loss. In addition it is the most complete simulation of scotomas in VR. In particular, the symptoms can be interactively modified and uniquely tuned to each patient's deficit. This enables a realistic simulation visual impairment the development of novel perceptual and psychophysical tests. In the future, we would like to conduct experiments with patients with well defined scotoma and quantify the performance of the proposed system in visual function recovery and perceptual compensation. Moreover, we can use bayesian distribution to iteratively update the model parameters over a number of trials to give a prediction on the future state of the parameters. This will be a very useful feature in disease screening and monitoring.

A similar model can be used for all of the other visual function tests. For example, modeling visual acuity with a fixed set of parameters would provide a more statistically based measure on the current and future values of minimum angle of resolution. When contrast sensitivity, dynamic visual acuity and more tests can be parameterized in a similar fashion the collective model of the visual system would be considerably more informative and may even result in a VR-based perceptual simulation that can be easily verified. Such a multidimensional representation of the human visual system would surely prove to be an indispensable tool for perceptually-based diagnostics.

In addition, we plan to include vernier acuity, color and depth sensitivity to the visual tests administered by this system.

The proposed VR-based assessment system would have the potential for use in remote environments with limited access to ophthalmic expertise and resource to make measurements of the visual function. The functional assessments could be used in conjunction with AI/ML approaches to help remotely diagnose retinal disorders [83, 84], improve the accuracy and transferrability of the results of traditional tests [85], or in fusion models for multi-modal processing of ophthalmic data [86–89].

6.3 Conclusion

This research provides a starting point for various future works and more in-depth studies. First of all, the conducted project could be repeated with a larger sample of people divided into different categories according to their various deficits. With a larger number of participants in which most of the dioptres', contrast range are represented, it would be possible to investigate if the results obtained in this thesis occur also on a larger scale or if they are just a coincidence.

A similar study as the one of this thesis could be conducted with astigmatic

or far-sighted subjects. The fascinating aspect of this research is represented by the suggestion that far-sighted users would not need corrective lenses when using an HMD. Accordingly, their VA would be higher in VR. Therefore, a comparison between these various groups of people could lead to a better understanding of HMDs and their impact on people with visual defects.

Chapter 7

Appendix

Table 7.1: Menu Screen

	Key	Function
1	Page Up	Move up the menu
2	Page Down	Move down menu
3	Enter	Start the selected assessment
4	Backspace	Go back to start screen
5	R	Show the visual assessment results for the current subject
6	Escape	Exit the Program

Table 7.2: Response in Static and Dynamic VA test

	Key	Function
1	9,8,7,4,1,2,3,6 Num Keys	Respond to landolt ring gap ↗, ↑, ↖, ←, ↙, ↓, ↘, →
2	Enter	Terminate test and go to results
3	Backspace	Go back to menu screen
4	Escape	Exit the Program

Table 7.3: Response in CS test

	Key	Function
1	9,8,7,6 Num Keys	Respond to landolt ring gap ↗, ↑, ↖, →
2	Enter	Terminate test and go to results
3	Backspace	Go back to menu screen
4	Escape	Exit the Program

Table 7.4: Various manipulations for a scotoma

	Key	Function
1	Page Up	Left Eye has Scotoma
2	Page Down	Right Eye has Scotoma
3	Left and Right Arrow	Cycle through the parameters
4	Up and Down Arrow	Change parameter values
5	8, 2, 4, 6 Num Keys	Move selected Scotoma ↑, ↓, ←, →
6	Tab	Add a new Scotoma
7	Space	Cycle through Scotoma

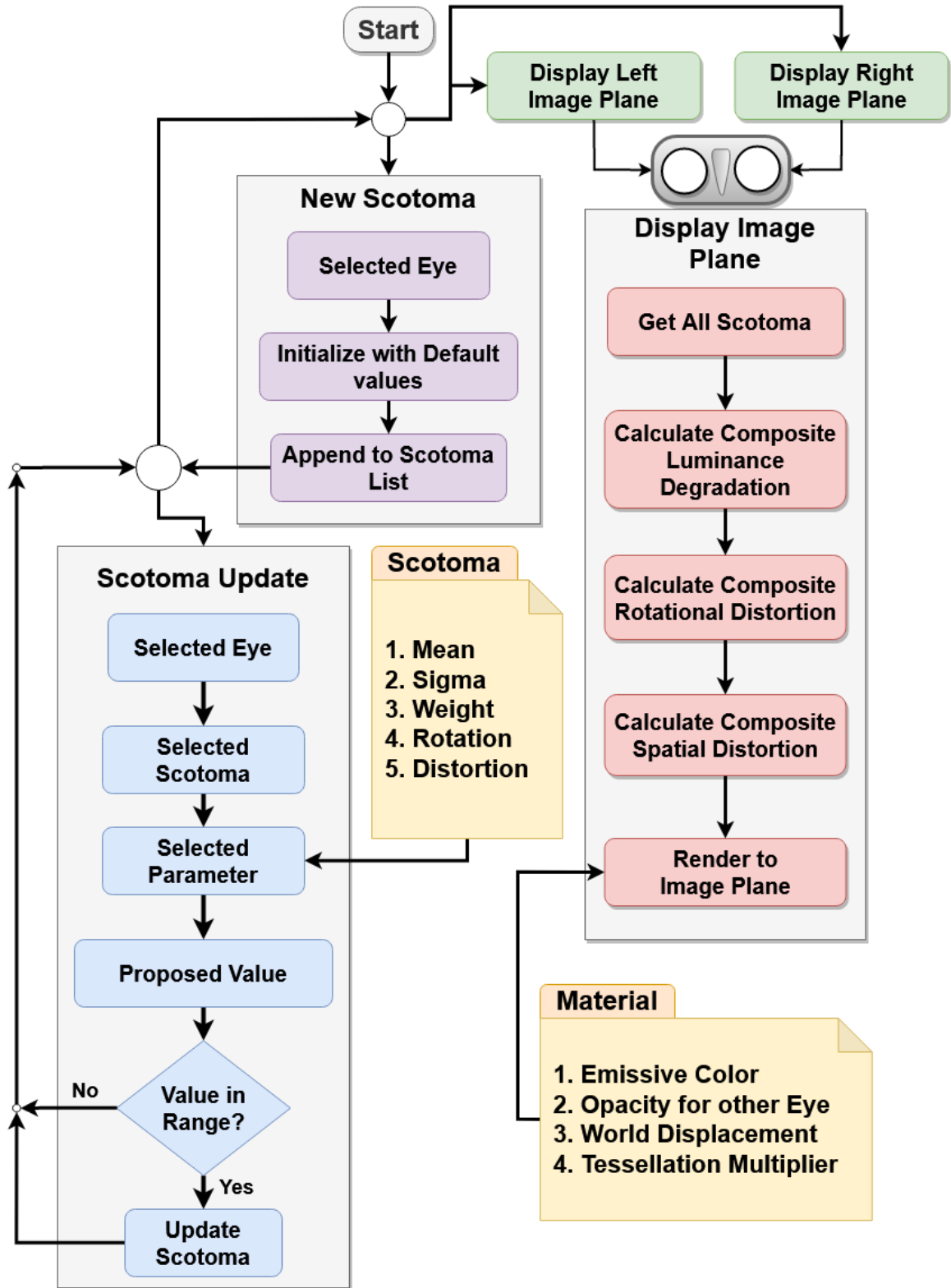
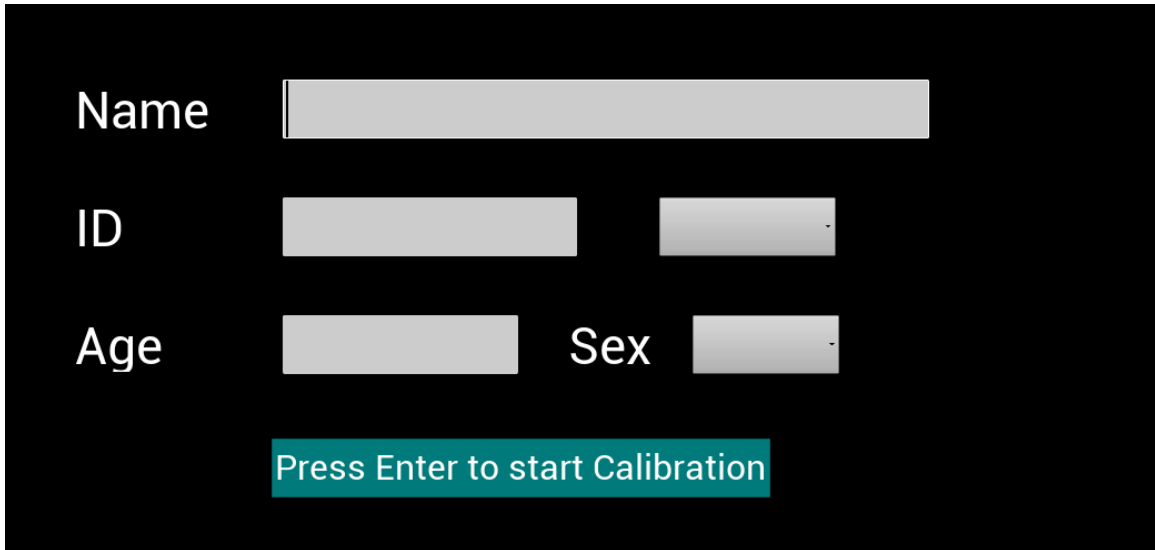


Figure 7.1: Overview of the Metamorphopsia Implementation



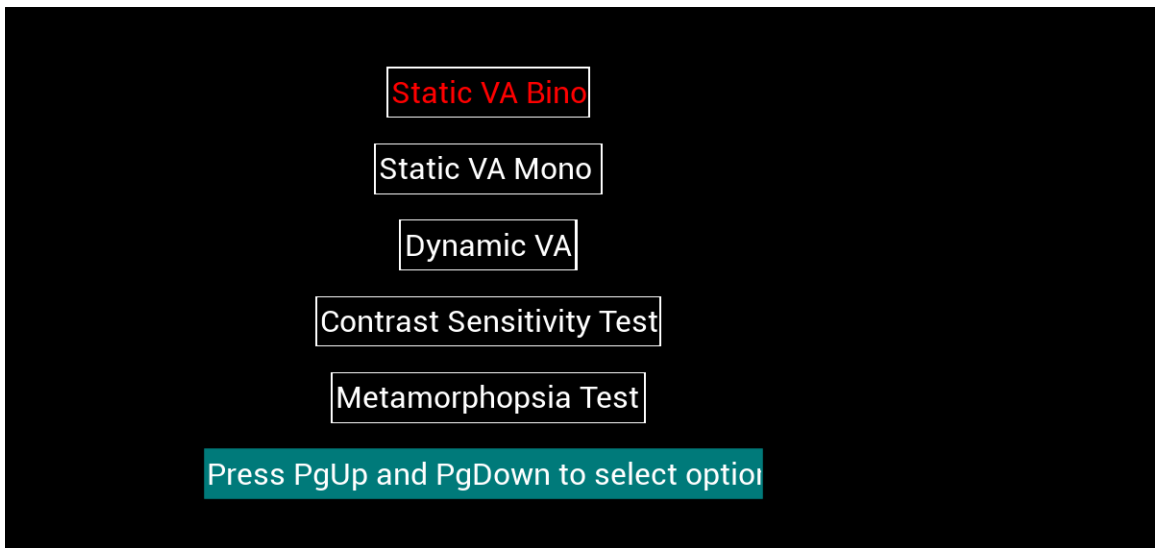
Name

ID

Age Sex

Press Enter to start Calibration

Figure 7.2: Start Screen



Static VA Bino

Static VA Mono

Dynamic VA

Contrast Sensitivity Test

Metamorphopsia Test

Press PgUp and PgDown to select option

Figure 7.3: Main Menu

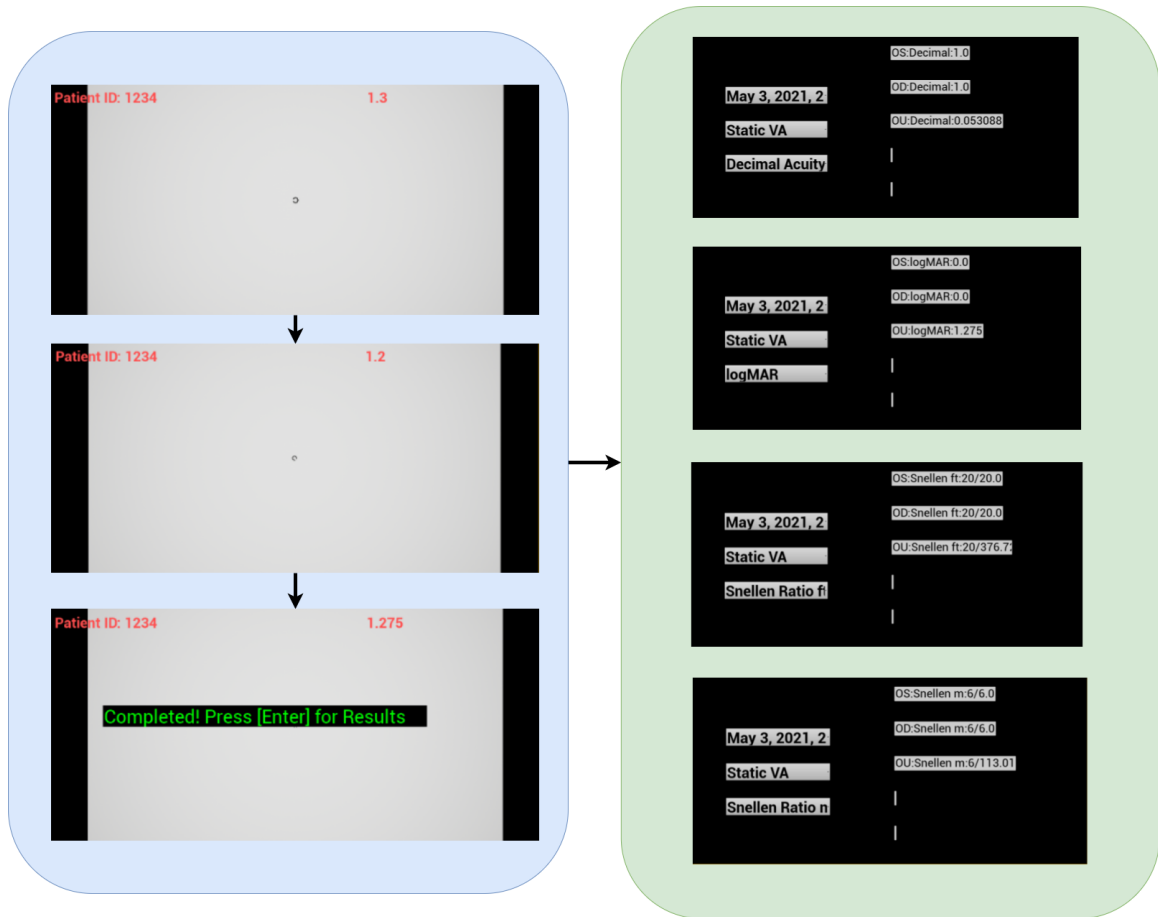


Figure 7.4: Binocular Static Visual Acuity

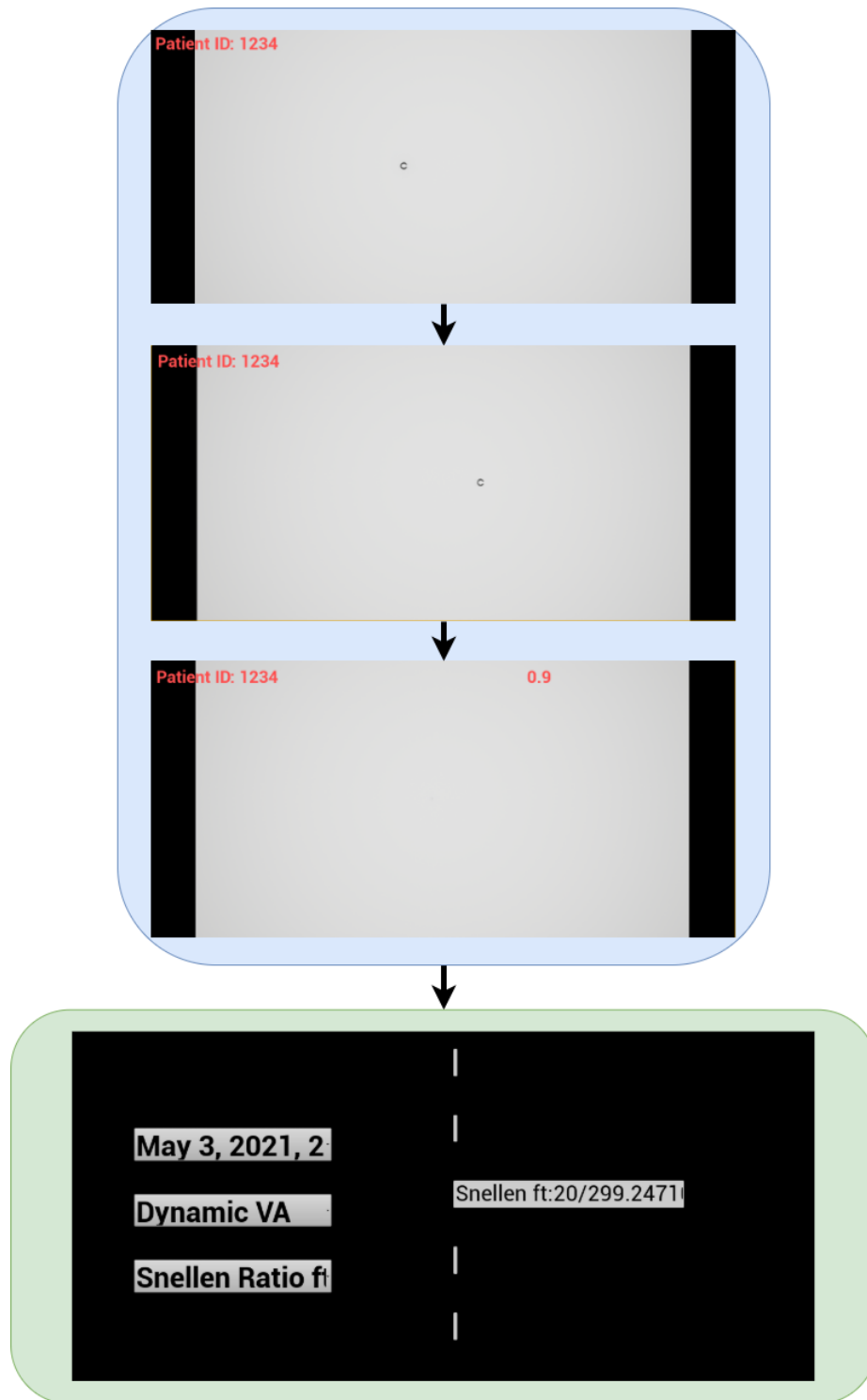


Figure 7.5: Binocular Dynamic Visual Acuity

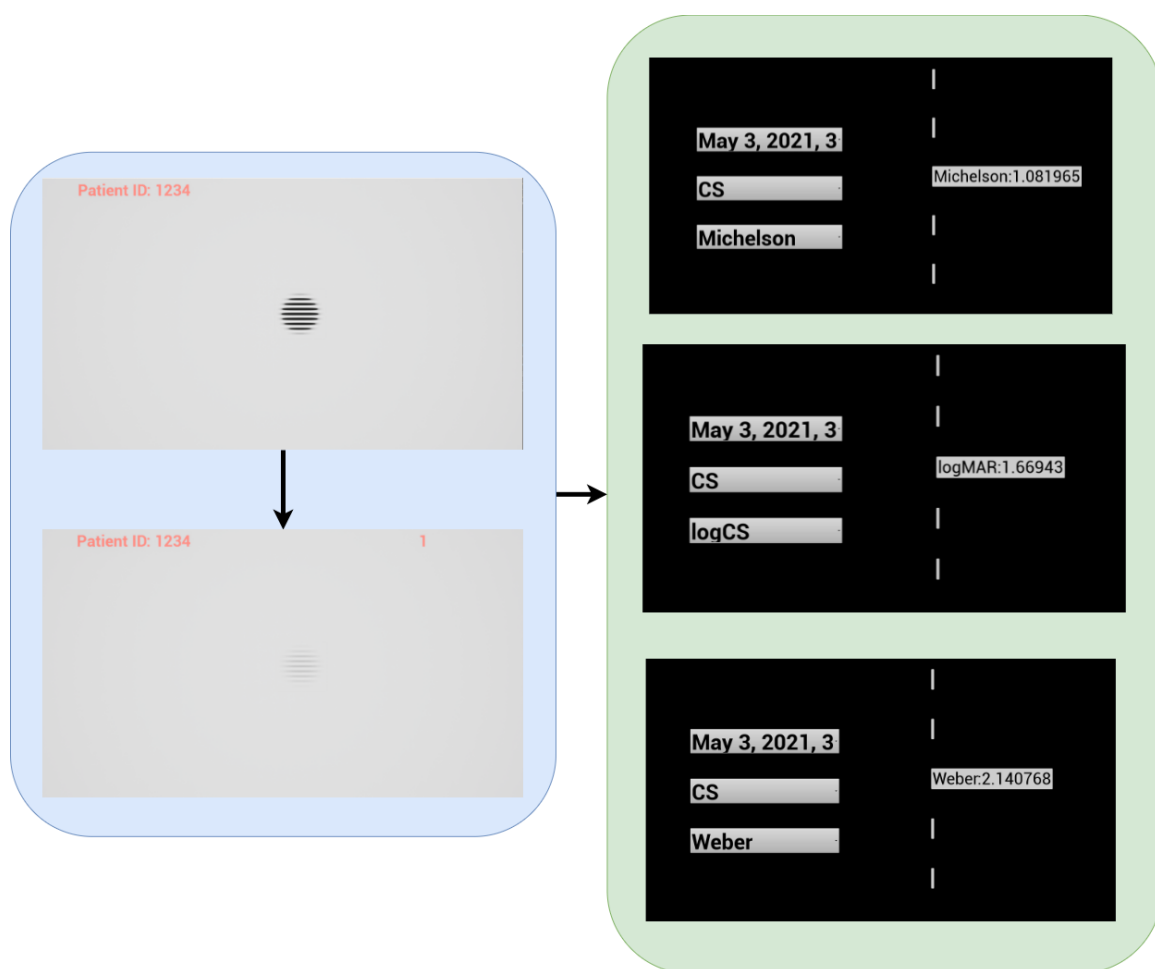


Figure 7.6: Contrast Sensitivity Test

Bibliography

- [1] “Cheat sheet.” [Online]. Available: <https://michaelbach.de/sci/acuity.html>
- [2] M. W. Gensheimer, M. B. Davies, L. C. J. Ellis, C. E. Chou, U. C. Cousineau-Krieger, M. J. Corsini, L. C. M. Caldwell, and C. S. A. Shackelford, “Eye trauma: Initial care (cpg id: 03),” *Joint Trauma System Clinical Practice Guideline*, 2020.
- [3] L. Kuzmiene, “Static perimetry,” pp. 109–113, 2019.
- [4] J. Capri, H. McLeod, L. V. Messner, A. S. Hariprasad, and D. Leong, “Color contrast sensitivity in age-related macular degeneration (amd),” *Investigative Ophthalmology & Visual Science*, vol. 59, no. 9, pp. 2418–2418, 2018.
- [5] M. Kaido, “Functional visual acuity,” *Investigative ophthalmology & visual science*, vol. 59, no. 14, pp. DES29–DES35, 2018.
- [6] J. A. Marron and I. L. Bailey, “Visual factors and orientation-mobility performance.” *American journal of optometry and physiological optics*, vol. 59, no. 5, pp. 413–426, 1982.
- [7] M. J. Moseley and A. R. Hill, “Contrast sensitivity testing in clinical practice.” *The British journal of ophthalmology*, vol. 78, no. 10, p. 795, 1994.
- [8] P. Scarfe and A. Glennerster, “The science behind virtual reality displays,” *Annual review of vision science*, vol. 5, pp. 529–547, 2019.

- [9] C. Blakemore and B. Julesz, "Stereoscopic depth aftereffect produced without monocular cues," *Science*, vol. 171, no. 3968, pp. 286–288, 1971.
- [10] J. M. Harris, "Binocular vision: moving closer to reality," *Philosophical Transactions of the Royal Society of London. Series A: Mathematical, Physical and Engineering Sciences*, vol. 362, no. 1825, pp. 2721–2739, 2004.
- [11] J. J. Koenderink and A. J. van Doorn, "Representation of local geometry in the visual system," *Biological cybernetics*, vol. 55, no. 6, pp. 367–375, 1987.
- [12] C. J. Bohil, B. Alicea, and F. A. Biocca, "Virtual reality in neuroscience research and therapy," *Nature reviews neuroscience*, vol. 12, no. 12, pp. 752–762, 2011.
- [13] M. C. Howard, "A meta-analysis and systematic literature review of virtual reality rehabilitation programs," *Computers in Human Behavior*, vol. 70, pp. 317–327, 2017.
- [14] M. Rus-Calafell, P. Garety, E. Sason, T. J. Craig, and L. R. Valmaggia, "Virtual reality in the assessment and treatment of psychosis: a systematic review of its utility, acceptability and effectiveness," *Psychological medicine*, vol. 48, no. 3, pp. 362–391, 2018.
- [15] G. Dagnelie, "Age-related psychophysical changes and low vision," *Investigative Ophthalmology & Visual Science*, vol. 54, no. 14, pp. ORSF88–ORSF93, 2013.
- [16] A. Achiron, O. Lagstein, M. Glick, Z. Gur, E. Bartov, and Z. Burgansky-Eliash, "Quantifying metamorphopsia in patients with diabetic macular oedema and other macular abnormalities," *Acta ophthalmologica*, vol. 93, no. 8, pp. e649–e653, 2015.
- [17] A. Colenbrander, "Visual standards aspects and ranges of vision loss with emphasis on population surveys," *International Council of Ophthalmology*, 01 2002.

- [18] W. Benjamin, “Borish’s clinical refraction: Monocular and binocular subjective refraction by borish im,” 2006.
- [19] A. B. Watson and A. J. Ahumada, “A standard model for foveal detection of spatial contrast,” *Journal of vision*, vol. 5, no. 9, pp. 6–6, 2005.
- [20] E. Wiecek, S. C. Dakin, and P. Bex, “Metamorphopsia and letter recognition,” *Journal of vision*, vol. 14, no. 13, pp. 27–27, 2014.
- [21] K. Tripathy and B. Salini, “Amsler grid,” *StatPearls [Internet]*, 2020.
- [22] D. T. Nguyen, A. Fahimi, W. Fink, P. P. Nazemi, J. K. Kim, and A. A. Sadun, “Novel 3d computer-automated threshold amsler grid visual field testing of scotomas in patients with glaucoma,” *European journal of ophthalmology*, vol. 19, no. 5, pp. 776–782, 2009.
- [23] R. L. Brown and A. E. Barrett, “Visual impairment and quality of life among older adults: an examination of explanations for the relationship,” *Journals of Gerontology Series B: Psychological Sciences and Social Sciences*, vol. 66, no. 3, pp. 364–373, 2011.
- [24] R. Bourne, J. D. Steinmetz, S. Flaxman, P. S. Briant, H. R. Taylor, S. Resnikoff, R. J. Casson, A. Abdoli, E. Abu-Gharbieh, A. Afshin *et al.*, “Trends in prevalence of blindness and distance and near vision impairment over 30 years: an analysis for the global burden of disease study,” *The Lancet Global Health*, 2020.
- [25] K. S. Naidoo, T. R. Fricke, K. D. Frick, M. Jong, T. J. Naduvilath, S. Resnikoff, and P. Sankaridurg, “Potential lost productivity resulting from the global burden of myopia: systematic review, meta-analysis, and modeling,” *Ophthalmology*, vol. 126, no. 3, pp. 338–346, 2019.

- [26] T. J. Heesterbeek, H. P. van der Aa, G. H. van Rens, J. W. Twisk, and R. M. van Nispen, “The incidence and predictors of depressive and anxiety symptoms in older adults with vision impairment: a longitudinal prospective cohort study,” *Ophthalmic and Physiological Optics*, vol. 37, no. 4, pp. 385–398, 2017.
- [27] S. Hodge and F. Eccles, “Loneliness, social isolation and sight loss,” *Retrieved from Lancaster University, Division of Health Research website: <http://googl/T8GDDB>*, 2013.
- [28] B. K. Swenor, B. Muñoz, and S. K. West, “A longitudinal study of the association between visual impairment and mobility performance in older adults: the salisbury eye evaluation study,” *American journal of epidemiology*, vol. 179, no. 3, pp. 313–322, 2014.
- [29] P. Loriaut, P. Loriaut, P. Boyer, P. Massin, and I. Cochereau, “Visual impairment and hip fractures: a case-control study in elderly patients,” *Ophthalmic research*, vol. 52, no. 4, pp. 212–216, 2014.
- [30] C. Owsley, G. McGwin, K. Scilley, G. C. Meek, A. Dyer, and D. Seker, “The visual status of older persons residing in nursing homes,” *Archives of Ophthalmology*, vol. 125, no. 7, pp. 925–930, 2007.
- [31] A. G. Lee, T. H. Mader, C. R. Gibson, W. Tarver, P. Rabiei, R. F. Riascos, L. A. Galdamez, and T. Brunstetter, “Spaceflight associated neuro-ocular syndrome (sans) and the neuro-ophthalmologic effects of microgravity: a review and an update,” *npj Microgravity*, vol. 6, no. 1, pp. 1–10, 2020.
- [32] “Medical eye exams during spaceflight.” [Online]. Available: https://lsda.jsc.nasa.gov/lsda_data/document/Project/MRID/MEDB_1.10_1.10.1_Eye%20Examinations%2012_11_17_Project_13_27_17.pdf

- [33] T. M. Appelboom, “A history of vision screening,” *Journal of school health*, vol. 55, no. 4, pp. 138–141, 1985.
- [34] A. T. Chuang, C. E. Margo, and P. B. Greenberg, “Retinal implants: a systematic review,” *British Journal of Ophthalmology*, vol. 98, no. 7, pp. 852–856, 2014.
- [35] G. Dagnelie, “Why aren’t retinal prostheses as good as cochlear implants, and what can we do to change that?” *Optical Society of America Fall Vision Conference*, 2018.
- [36] P. Kalanithi and D. Purger, “Chapter 6 - optogenetics,” in *Innovative Neuromodulation*, J. Arle and J. Shils, Eds. San Diego: Academic Press, 2017, pp. 123 – 134.
- [37] S. Fried and S. Lee, “Towards a micro-coil based cortical visual prosthesis,” *Optical Society of America Fall Vision Conference*, 2017.
- [38] D. R. Lampton, B. W. Knerr, S. L. Goldberg, J. P. Bliss, J. M. Moshell, and B. S. Blau, “The virtual environment performance assessment battery (vepab): Development and evaluation,” *Presence: Teleoperators & Virtual Environments*, vol. 3, no. 2, pp. 145–157, 1994.
- [39] D. Maxwell, E. Oster, S. Lynch, D. Maxwell, E. Oster, and S. Lynch, “Evaluating the applicability of repurposed entertainment virtual reality devices for military training,” *MODSIM World*, p. 0028, 2018.
- [40] D. Sproule, R. F. Jacinto, S. Rundell, J. Williams, S. Perlmutter, and S. Arndt, “Characterization of visual acuity and contrast sensitivity using head-mounted displays in a virtual environment: A pilot study,” *Proceedings of the Human Factors and Ergonomics Society Annual Meeting*, vol. 63, no. 1, pp. 547–551, 2019.

- [41] L. Panfili, "Effects of vr-displays on visual acuity," 2019.
- [42] S. C. Ong, L. C. I. Pek, T. L. C. Chiang, H. W. Soon, K. C. Chua, C. Sassmann, M. A. B. Razali, and T. C. V. Koh, "A novel automated visual acuity test using a portable head-mounted display," *Optometry and Vision Science*, vol. 97, no. 8, pp. 591–597, 2020.
- [43] J. De Letter, A. All, L. De Marez, V. Avramelos, P. Lambert, and G. Van Wallendaël, "Exploratory study on user's dynamic visual acuity and quality perception of impaired images," *arXiv preprint arXiv:2001.03542*, 2020.
- [44] P. Aniruddha, N. Zaman, A. Tavakkoli, and S. Zuckerbrod, "A parametric perceptual deficit modeling and diagnostics framework for retina damage using mixed reality," *International Symposium on Visual Computing*, pp. 258–269, 2019.
- [45] N. Zaman, A. Tavakkoli, and S. Zuckerbrod, "A mixed reality system for modeling perceptual deficit to correct neural errors and recover functional vision," *2020 IEEE Conference on Virtual Reality and 3D User Interfaces Abstracts and Workshops (VRW)*, pp. 269–274, 2020.
- [46] D. B. Elliott, "Clinical procedures in primary eye care e-book," 2013.
- [47] G. Tidow, K. WUHST, and H. DEMAREES, "Dynamic visual-acuity as a performance-influencing factor in sport," in *International Journal of Sports Medicine*, vol. 5, no. 5. GEORG THIEME VERLAG PO BOX 30 11 20, D-70451 STUTTGART, GERMANY, 1984, pp. 296–296.
- [48] N. R. Council *et al.*, *Emergent techniques for assessment of visual performance*. National Academies Press, 1985.
- [49] G. M. Long and D. F. Kearns, "Visibility of text and icon highway signs under dynamic viewing conditions," *Human factors*, vol. 38, no. 4, pp. 690–701, 1996.

- [50] S. A. Kelly, Y. Pang, and S. Klemencic, "Reliability of the csv-1000 in adults and children," *Optometry and Vision Science*, vol. 89, no. 8, pp. 1172–1181, 2012.
- [51] B. P. Rosenthal and M. Fischer, "Functional vision changes in the normal and aging eye," *A comprehensive guide to geriatric rehabilitation*, pp. 381–391, 2014.
- [52] A. W. Scott, N. M. Bressler, S. Ffolkes, J. S. Wittenborn, and J. Jorkasky, "Public attitudes about eye and vision health," *JAMA ophthalmology*, vol. 134, no. 10, pp. 1111–1118, 2016.
- [53] D. S. Fong, M. Sharza, W. Chen, J. F. Paschal, R. G. Ariyasu, and P. P. Lee, "Vision loss among diabetics in a group model health maintenance organization (hmo)," *American journal of ophthalmology*, vol. 133, no. 2, pp. 236–241, 2002.
- [54] S. M. Saw, G. Gazzard, D. Friedman, P. Foster, J. Devereux, M. Wong, and S. Seah, "Awareness of glaucoma, and health beliefs of patients suffering primary acute angle closure," *British journal of ophthalmology*, vol. 87, no. 4, pp. 446–449, 2003.
- [55] J. Lau, V. Lee, D. Fan, M. Lau, and J. Michon, "Knowledge about cataract, glaucoma, and age related macular degeneration in the hong kong chinese population," *British journal of ophthalmology*, vol. 86, no. 10, pp. 1080–1084, 2002.
- [56] K. Mansouri, S. Orgül, F. Meier-Gibbons, and A. Mermoud, "Awareness about glaucoma and related eye health attitudes in switzerland: a survey of the general public," *Ophthalmologica*, vol. 220, no. 2, pp. 101–108, 2006.
- [57] M. Katibeh, H. Ziaei, E. Panah, H.-R. Moein, S. Hosseini, M. Kalantarion, A. Eskandari, and M. Yaseri, "Knowledge and awareness of age related eye diseases: a population-based survey," *Journal of ophthalmic & vision research*, vol. 9, no. 2, p. 223, 2014.

- [58] U. Altangerel, H. S. Nallamshetty, T. Uhler, J. Fontanarosa, W. C. Steinmann, J. M. Almodin, B. H. Chen, and J. D. Henderer, “Knowledge about glaucoma and barriers to follow-up care in a community glaucoma screening program,” *Canadian Journal of Ophthalmology*, vol. 44, no. 1, pp. 66–69, 2009.
- [59] D. Shickle and M. Griffin, “Why don’t older adults in england go to have their eyes examined?” *Ophthalmic and Physiological Optics*, vol. 34, no. 1, pp. 38–45, 2014.
- [60] J. G. Lawrenson, E. Graham-Rowe, F. Lorencatto, J. Burr, C. Bunce, J. J. Francis, P. Aluko, S. Rice, L. Vale, T. Peto *et al.*, “Interventions to increase attendance for diabetic retinopathy screening,” *Cochrane Database of Systematic Reviews*, no. 1, 2018.
- [61] A. Müller, J. E. Keeffe, and H. R. Taylor, “Changes in eye care utilization following an eye health promotion campaign,” *Clinical & experimental ophthalmology*, vol. 35, no. 4, pp. 305–309, 2007.
- [62] G. C. Brown, M. M. Brown, and S. Sharma, “Difference between ophthalmologists’ and patients’ perceptions of quality of life associated with age-related macular degeneration,” *Canadian Journal of Ophthalmology*, vol. 35, no. 3, pp. 127–133, 2000.
- [63] M. Maxhall, A. Backman, K. Holmlund, L. Hedman, B. Sondell, and G. Bucht, “Participants responses to a stroke training simulator,” *Proc. of ICDVRAT*, vol. 4, 2002.
- [64] B. Jin, Z. Ai, and M. Rasmussen, “Simulation of eye disease in virtual reality,” *2005 IEEE engineering in medicine and biology 27th annual conference*, pp. 5128–5131, 2006.

- [65] R. Velázquez, C. N. Sánchez, and E. E. Pissaloux, “Visual impairment simulator based on the hadamard product.” *CLEI Selected Papers*, pp. 169–179, 2016.
- [66] F. Werfel, R. Wiche, J. Feitsch, and C. Geiger, “Empathizing audiovisual sense impairments: Interactive real-time illustration of diminished sense perception,” *Proceedings of the 7th Augmented Human International Conference 2016*, pp. 1–8, 2016.
- [67] D. Randall, H. Griffiths, G. Arblaster, A. Bjerre, and J. Fenner, “Simulation of oscillopsia in virtual reality,” *British and Irish Orthoptic Journal*, vol. 14, no. 1, pp. 45–49, 2018.
- [68] K. E. Wolffe and A. R. Candela, “A qualitative analysis of employers’ experiences with visually impaired workers,” *Journal of Visual Impairment & Blindness*, vol. 96, no. 9, pp. 622–634, 2002.
- [69] A. Crudden, L. W. McBroom, A. L. Skinner, and J. E. Moore, “Comprehensive examination of barriers to employment among persons who are blind or visually impaired.” 1998.
- [70] S. J. La Grow and P. Daye, “Barriers to employment identified by blind and vision-impaired persons in new zealand,” *Social Policy Journal of New Zealand*, vol. 26, p. 173, 2005.
- [71] M. C. McDonnall, J. O’Mally, and A. Crudden, “Employer knowledge of and attitudes toward employees who are blind or visually impaired,” *Journal of Visual Impairment & Blindness*, vol. 108, no. 3, pp. 213–225, 2014.
- [72] D. Papakonstantinou and K. Papadopoulos, “The impact of information on employers’ attitudes towards employees with visual impairments,” *Journal of Vocational Rehabilitation*, vol. 47, no. 1, pp. 99–107, 2017.

- [73] K. A. Lynch, “Survey reveals myths and misconceptions abundant among hiring managers about the capabilities of people who are visually impaired,” *Journal of Visual Impairment & Blindness*, vol. 107, no. 6, pp. 408–410, 2013.
- [74] S. Wang, M. Moharrer, V. Baliutaviciute, B. E. Dougherty, W. Cybis, A. R. Bowers, and G. Luo, “Bioptic telescope use in naturalistic driving by people with visual impairment,” *Translational Vision Science & Technology*, vol. 9, no. 4, pp. 11–11, 2020.
- [75] M. Moharrer, S. Wang, B. E. Dougherty, W. Cybis, B. R. Ott, J. D. Davis, and G. Luo, “Evaluation of the driving safety of visually impaired bioptic drivers based on critical events in naturalistic driving,” *Translational Vision Science & Technology*, vol. 9, no. 8, pp. 14–14, 2020.
- [76] P. R. Jones and G. Ometto, “Degraded reality: using vr/ar to simulate visual impairments,” *2018 IEEE Workshop on Augmented and Virtual Realities for Good (VAR4Good)*, pp. 1–4, 2018.
- [77] S. Stock, C. Erler, and W. Stork, “Realistic simulation of progressive vision diseases in virtual reality,” *Proceedings of the 24th ACM Symposium on Virtual Reality Software and Technology*, pp. 1–2, 2018.
- [78] K. Krösl, C. Elvezio, M. Hürbe, S. Karst, S. Feiner, and M. Wimmer, “Xreye: Simulating visual impairments in eye-tracked xr,” *2020 IEEE Conference on Virtual Reality and 3D User Interfaces Abstracts and Workshops (VRW)*, pp. 831–832, 2020.
- [79] A. Johnson, M. Allen, R. Pryzby, R. Wright, S. Robison, and X. Scrimgeour, “See what i see: Virtual reality eye disease experience,” 2020. [Online]. Available: <https://>

[//www.nei.nih.gov/learn-about-eye-health/resources-for-health-educators/see-what-i-see-virtual-reality-eye-disease-experience](https://www.nei.nih.gov/learn-about-eye-health/resources-for-health-educators/see-what-i-see-virtual-reality-eye-disease-experience)

- [80] M. Bach, “The freiburg visual acuity test-variability unchanged by post-hoc re-analysis,” *Graefe’s Archive for Clinical and Experimental Ophthalmology*, vol. 245, no. 7, pp. 965–971, 2006.
- [81] S. Coren and C. P. Kaplan, “Patterns of ocular dominance,” *Optometry and Vision Science*, vol. 50, no. 4, pp. 283–292, 1973.
- [82] L. Thevin and T. Machulla, “Guidelines for inclusive avatars and agents: How persons with visual impairments detect and recognize others and their activities,” in *International Conference on Computers Helping People with Special Needs*. Springer, 2020, pp. 164–175.
- [83] S. A. Kamran, S. Saha, A. S. Sabbir, and A. Tavakkoli, “A comprehensive set of novel residual blocks for deep learning architectures for diagnosis of retinal diseases from optical coherence tomography images,” in *Deep Learning Applications, Volume 2*. Springer, 2021, pp. 25–48.
- [84] —, “Optic-net: A novel convolutional neural network for diagnosis of retinal diseases from optical tomography images,” in *2019 18th IEEE International Conference On Machine Learning And Applications (ICMLA)*. IEEE, 2019, pp. 964–971.
- [85] S. A. Kamran, A. Tavakkoli, and S. L. Zuckerbrod, “Improving robustness using joint attention network for detecting retinal degeneration from optical coherence tomography images,” in *2020 IEEE International Conference On Image Processing (ICIP)*. IEEE, 2020, pp. 2476–2480.

- [86] S. A. Kamran, K. F. Hossain, A. Tavakkoli, S. Zuckerbrod, S. A. Baker, and K. M. Sanders, “Fundus2angio: A conditional gan architecture for generating fluorescein angiography images from retinal fundus photography,” in *International Symposium on Visual Computing*. Springer, 2020, pp. 125–138.
- [87] A. Tavakkoli, S. A. Kamran, K. F. Hossain, and S. L. Zuckerbrod, “A novel deep learning conditional generative adversarial network for producing angiography images from retinal fundus photographs,” *Scientific Reports*, vol. 10, no. 1, pp. 1–15, 2020.
- [88] S. A. Kamran, K. F. Hossain, A. Tavakkoli, S. L. Zuckerbrod, K. M. Sanders, and S. A. Baker, “Vtgan: Semi-supervised retinal image synthesis and disease prediction using vision transformers,” *arXiv preprint arXiv:2104.06757*, 2021.
- [89] —, “Rv-gan : Retinal vessel segmentation from fundus images using multi-scale generative adversarial networks,” 2021.